University of Alberta

Fabrication of Nanostructures in Nonlinear Optical Ionically Self-Assembled Monolayers

by

Aruna Lucille Kroetch ©

A thesis submitted to the Faculty of Graduate Studies and Research
in partial fulfillment of the requirements for the degree of

Master of Science

Department of Electrical and Computer Engineering

Edmonton, Alberta
Spring 2008

Your file Votre référence
ISBN: 978-0-494-45837-2
Our file Notre référence
ISBN: 978-0-494-45837-2

Abstract

There is a sustained interest towards the development of high quality and robust optical components that would enable a continued progression towards integrated photonic systems. In this context, organic thin films have been examined as candidates from which to fabricate photonic devices. Specifically, ionically self-assembled monolayer (ISAM) films represent a material platform that combines nonlinear optical properties that can be exploited to create active photonic devices, with a polymeric nature which is conducive to polymer-based manufacturing. This thesis investigates the fabrication methodology needed to create photonic structures in PCBS/PAH ISAM films using both reactive ion etch and nanoimprint lithography techniques.

Acknowledgements

First, it is my priviledge to acknowledge my advisor, Dr. Stephane Evoy. Thank you for providing this opportunity to work on this project Our conversations always provided insight on my project and really honed my ability to evaluate the scope of its focus.

To my partner-in-crime, Steve Buswell, thanks for always being there to discuss random optic and fabrication ideas. I have often appreciated your ability to make sense of confusion.

I would also like to acknowledge my collaborators in Virginia. Cemil Durak, in Dr. Heflin's group at Virginia Tech, has been such a wonderful source of expertise and friendship during our collaboration. Thank you for training me on ISAM synthesis, for creating films when I was unable to, and for taking multiple SHG measurements for me. I cannot express enough gratitude for consistently providing transportation at midnight to change solutions. Your kindness and commitment will never be forgotten. I would also like to thank Dr. Randy Heflin who always made time to answer my questions and enabled me to gain so much practical knowledge on ISAM films when I was visiting Virginia. I would like to acknowledge Vladimir Kochergin at Luna Innovations Inc., who went out of his way to ensure my trip to Virginia and this project were successful. A special

thanks to Jason Ridley who also so kindly picked me multiple times at midnight so that I could change solutions.

I cannot fail to acknowledge the staff at the University of Alberta's NanoFab, especially Dr. Ken Westra who introduced me to the world of microfabrication and nanotechnology. Thanks to all of the staff members at the NanoFab for providing me with invaluable knowledge and laughter. Daniel Salomon, at the National Institute for Nanotechnology (NINT), deserves my appreciation for all his assistance with scanning electron microscopy.

I would also like to thank Andrew Murray for keeping it interesting at our desk and Prakriti Parijat who was the best roommate I could have asked for. Thanks to Luc Gervais for your atomic force microscopy expertise and Neal Wilding for training my on FTIR.

To my parents, who have supported me in every path I have taken, I cannot thank you enough for continuously helping me live up to my potential. Finally, I wish to thank my husband, Rob, for being there for me and with me every step of the way. I am consistently amazed at how lucky I got with you.

Contents

1 Introduction 1

1.1 Nanoimprint Lithography 2

1.2 Photonic Structures 5

1.3 Nonlinear Optics 5

1.4 Overview 9

2 Organic Thin Film Deposition 10

2.1 Poled Polymers 11

2.2 Langmuir-Blodgett Films 14

2.3 Covalent Self-Assembled Monolayers 15

2.4 Summary 16

3 Ionically Self-Assembled Monolayers 17

3.1 Inherent Traits 18

3.2 Origin of Nonlinear Optical ISAM Films 21

3.3 Applications 24

3.4 Patterning ISAM Films 26

3.5 Summary 28

4 Synthesis and Characterization of ISAM Films 29

4.1 Experimental Details 30

4.1.1 Materials 30

4.1.2 Dipping Process 32

4.1.3 Characterization Equipments 33

4.2 Characterization 34

4.2.1 Topography 34

4.2.2 Thermal Stability 37

4.3 Summary 41

5 Lithography-Based Fabrication of ISAM Films 42

5.1 Experimental Details 43

5.1.1 Materials 43

5.1.2 Fabrication Details 44

5.1.3 Optical Waveguide Testing Apparatus 46

5.2 Development of a Polymer Fabrication Process – Phase 1 47

5.3 Patterning ISAM Films – Phase 2 49

5.4 Hybrid ISAM/Si Waveguides – Phase 3 55

5.5 Summary 57

6 Nanoimprint Lithography of ISAM Films 59
6.1 Experimental Details 60
6.1.1 Materials 60
6.1.2 Fabrication Details 61
6.1.3 Optical Characterization 63
6.2 Development of Nanoimprint Molds – Phase 1 64
6.3 NIL in PMMA – Phase 2 67
6.4 NIL in ISAM Films – Phase 3..... 69
6.5 Summary 73
7 Conclusion 74
8 Bibliography 80

List of Tables

Table 4.1: Percent mass concentration of PCBS/PAH ISAM films 40
after being heated to different temperatures and cooled
back to room temperature.

Table 5.1: Chemicals used in patterning ISAM films with lithography 43

Table 6.1: Chemicals used in patterning ISAM films with 60
nanoimprint lithography.

List of Figures

Figure 1.1: Nanoimprint lithography process..... 3

Figure 1.2: Photonic crystal structure with 10 nm hole diameter] 4

Figure 2.1: Chromophore alignment before and after poling 11

Figure 2.2: Langmuir-Blodgett deposition technique..... 14

Figure 3.1: Ionically self-assembled monolayer deposition technique 20

Figure 4.1: Structural formula of the polyelectrolytes 32

Figure 4.2: Richard-Allen Scientific DS/50 automated slide stainer 33

Figure 4.3: Topography and inhomogeneous sites of ISAM films 35

Figure 4.4: AFM images of 500 bilayer PCBS/PAH ISAM film..... 36

Figure 4.5: FTIR spectra of PCBS/PAH films that have been heated 39
and then cooled back room temperature.

Figure 5.1: Optical test apparatus for guiding light in ISAM 47
Waveguides

Figure 5.2: Process flow for patterning photonic structures in 48
HPR 504, which was used as an ISAM
representative polymer.

Figure 5.3: Photonic crystal structures were patterned into HPR 504 49
films using an oxygen plasma.

Figure 5.4: Crack formation in ISAM films 50

Figure 5.5: Modified ISAM fabrication process flow 51

Figure 5.6: PCBS/PAH ISAM films patterned with optical lithography. 52

Figure 5.7: Photonic crystal structures fabricated in ISAM films using electron beam lithography. 54

Figure 5.8: Simple waveguides and Bragg gratings fabricated in ISAM films. 54

Figure 5.9: PCBS/PAH ISAM films waveguide film with both inhomogeneous sites and sidewall roughness 55

Figure 5.10: Process flow for the hybrid ISAM/Si photonic structures.....56

Figure 5.11: Hybrid ISAM/Si photonic crystals were fabricated..... 57

Figure 6.1: Second harmonic generation measurement apparatus. 64

Figure 6.2: Fabrication process for the creation of silicon molds 65

Figure 6.3: Etching profile typical of the deep silicon etching process 65

Figure 6.4: An uniform silicon imprinting mold created deep silicon etching process for micron scale imprinting. 66

Figure 6.5: Nanoimprint lithography molds created with electron beam lithography 67

Figure 6.6: Photonic structures imprinted in PMMA 68

Figure 6.7: First imprint in ISAM films with a nanometer-scale silicon mold. 69

Figure 6.8: Photonic crystal structures imprinted in PCBS/PAH ISAM films 70

Figure 6.9: Waveguide and Bragg gratings imprinted in ISAM films..... 71

Figure 6.10: Demonstrations of incomplete imprinting because of inhomogeneous sites. 72

Figure 6.11: Second harmonic generation of PCBS/PAH ISAM films after being imprinted with different fill factors. 73

Chapter 1

Introduction

There is a sustained interest towards the development of high quality and robust optical components that would enable the further integration of optical systems. Organic thin films have specifically been examined as promising candidates for the fabrication of nonlinear photonic devices. Specifically, ionically self-assembled monolayers (ISAM) represent a material platform offering nonlinear optical properties that can be exploited to create active photonic devices, as well as a polymeric nature that is conducive to cost-efficient manufacturing. This thesis investigates fabrication methodologies needed to create such photonic structures in ISAM films

Ionically self-assembled monolayers are simple and inexpensively fabricated, and offer excellent thermal and temporal stability. A negatively charged substrate is alternately dipped in polycation and polyanion solutions, resulting in a multilayer film that self-assembles due to the electrostatic interactions between each layer. Such assembly process is easily scaled and automated.

ISAM films are easily tailored by incorporating various materials, resulting in films that can be engineered to display different properties. In particular, ISAM films embedded with chromophores will display nonlinear optical properties [1,2]. This chromophore alignment causing these properties is tightly maintained by electrostatic interactions between the oppositely charged monolayers.

This project aimed to develop a platform enabling the patterning of ISAM films for eventual photonic crystals applications. More specifically, the polymeric nature of ISAM films makes them conducive to patterning by both reactive ion etching as well as by nanoimprint lithography

1.1 Nanoimprint Lithography

The inherent low cost of nanoimprint lithography (NIL) enables a commercially viable pathway for mass manufacturing of photonic and electronic devices [3]. This process provides high throughput and high uniformity to such manufacturing. Nanoimprint lithography (NIL) consists of physically deforming a thermoplastic polymer with a mold by applying a constant force at a temperature

exceeding its glass transition temperature. Under these conditions, the polymer flows and conformably contacts the mold. Demolding is then performed after the system temperature is lowered, resulting in an irreversible change in the topography of the imprinted polymer that is the negative image of the mold (Figure 1.1).

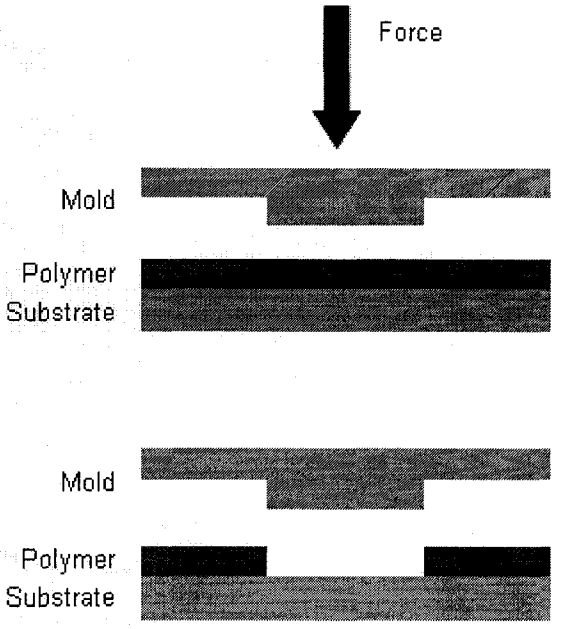

Figure 1.1: Nanoimprint lithography process.

Small dimensions can be achieved because NIL is not limited by diffraction or scattering like light-based lithography techniques. In addition, NIL is not prone to over etching issues encountered with wet etching [4,5]. This technique is readily conducive to the patterning of structures with features smaller than 10 nm (Figure 1.2) [4].

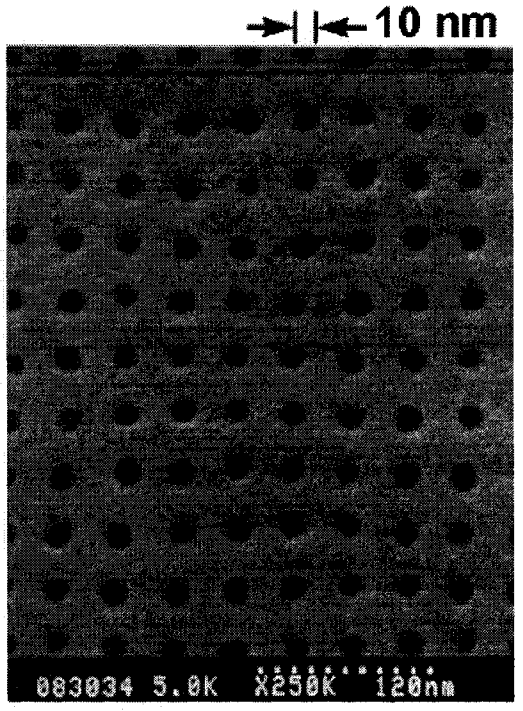

Figure 1.2: Pattern of 10 nm holes imprinted in PMMA using NIL [4].

In addition, typical dry etching methods employed in microfabrication results in some level of surface roughness that induce scattering losses [3]. NIL is a useful method to reduce scattering losses during optical guiding. The molds used in NIL can be smoothed with a simple oxide step, and therefore result in imprinted features offering smoother sidewalls. Several photonic structures have already been demonstrated realized using NIL, including microring resonators [3] and photonic crystal structures [5,6].

1.2 Photonic Structures

Photonic crystals and their photonic band gaps are analogous to semiconductors and their energy band gaps. The presence of these photonic band gaps results in a certain frequency range of electromagnetic waves that are prohibited from propagating in the structure [3,6-8]. This effect therefore enables the manipulation of the confinement of light.

In this work, both one-dimensional and two-dimensional photonic crystal structures will be used for proof of concept purposes. These structures can be realized by simply creating grating structures or air holes in a dielectric material, resulting in a periodic modulation of the dielectric constant. By incorporating line defects in the photonic crystal structure, a highly efficient waveguide can be produced where the light is confined in-plane by the photonic crystals and out-of-plane by total internal reflection [7].

1.3 Nonlinear Optics

In a linear isotropic media, the polarization density $\overline{P}$ is linearly related to its electric field $\overline{E}$ through:

$$\overline{P} = \varepsilon_o \chi \overline{E} \qquad (1.3.1)$$

where ε_o is the electric permittivity of free space and χ is the electric susceptibility. This linear approximation is valid for small electric fields in most materials. The displacement field $\overline{D}$ is also linearly related to the electric field by:

$$\overline{D} = \varepsilon \overline{E} \tag{1.3.2}$$

where ε is the dielectric constant, defined as

$$\varepsilon = \frac{\varepsilon_m}{\varepsilon_o} = \frac{\varepsilon_o(1+\chi)}{\varepsilon_o} = (1+\chi) \tag{1.3.3}$$

where ε_m is the electric permittivity in the medium.

As the electric field intensity increases, deviations from this linear response will occur. In such scenario, the polarization is expressed through a polynomial expansion:

$$\overline{P} = \varepsilon_o(\chi^{(1)}\overline{E} + \chi^{(2)}\overline{E}^2 + \chi^{(3)}\overline{E}^3 + ...) \tag{1.3.4}$$

where $\chi^{(1)}$ (equivalent to χ in (1.3.1)), represents the linear susceptibility, while all other coefficients, $\chi^{(n)}$ are the nth order nonlinear susceptibilities. If a material is centrosymmetric, such that it possesses an inversion symmetry, a reversal of $\overline{E}$ must result in a reversal of $\overline{P}$. For this to occur, the polarization density must possess an odd symmetry, and therefore cannot posses a second order susceptibility $\chi^{(2)}$. A material must therefore be noncentrosymmetric in order to display second order nonlinear behavior. This thesis focuses on fabrication of photonic devices in noncentrosymmetric polymeric films synthesized using an ionic self-assembly method.

Now, assuming that the incident electric field takes the form

$$\overline{E}(t) = E_o \cos(\omega t) \tag{1.3.5}$$

where E_o is the amplitude of the field and ω is the angular frequency.

Substituting in (1.3.2) gives

$$\begin{aligned} P &= \varepsilon_o(\chi^{(1)} E_o \cos(\omega t) + \chi^{(2)} E_o^2 \cos^2(\omega t) + \chi^{(3)} E_o^3 \cos^3(\omega t) + \ldots) \\ &= \tfrac{1}{2}\varepsilon_o \chi^{(2)} E_o^2 + \varepsilon_o(\chi^{(1)} + \tfrac{3}{4}\chi^{(3)} E_o^2) E_o \cos(\omega t) \\ &\quad + \tfrac{1}{2}\varepsilon_o \chi^{(2)} E_o^2 \cos(2\omega t) + \tfrac{1}{4}\varepsilon_o \chi^{(3)} E_o^3 \cos(3\omega t) \ldots \end{aligned} \tag{1.3.6}$$

Typically, $\chi^{(3)}$ is small and can be ignored in second order nonlinear optical materials. The first term is a constant representing the steady state contribution, while the following terms represent the fundamental, second, and third harmonic of polarization, respectively.

From (1.3.6), an incident field that interacts with a material that possesses a second order nonlinear susceptibility will display a component at twice the frequency. This phenomenon is referred to as second harmonic generation, and will scale with the constant $\chi^{(2)}$.

If the electric field in (1.3.5) has an additional steady state component E(0) added, given by

$$\overline{E} = E(0) + E_o \cos(\omega t) \tag{1.3.7}$$

and is substituted into the second order polarization given by:

$$\overline{P}^{(2)} = \varepsilon_o \chi^{(2)} \overline{E}^2 \tag{1.3.8}$$

then the second order polarization will become:

$$\begin{aligned} \overline{P}^{(2)} &= \varepsilon_o \chi^{(2)} \overline{E}^2 = \varepsilon_o \chi^{(2)} [E(0) + E_o \cos(\omega t)]^2 \\ &= \varepsilon_o \chi^{(2)} [\tfrac{1}{2} E_0^2 + E^2(0) + 2E(0)E_o \cos(\omega t) + \tfrac{1}{2} E_0^2 \cos(2\omega t)] \end{aligned} \tag{1.3.9}$$

A second harmonic component is again present through the 2ω term. However an electro-optic effect, or Pockels effect, arises in the ω term and results in a change of the refractive index of the material that scales linearly with the field. The index of refraction n of a material is given by:

$$n = \sqrt{\varepsilon} \tag{1.3.10}$$

And therefore, in a linear material:

$$n = \sqrt{(1+\chi)} \tag{1.3.11}$$

the index of refraction has no dependence on the incident electric field.

The refractive index of a second order nonlinear optical material n' is however given by:

$$n' = n + \frac{\chi^{(2)}}{n} E(0) = n - \tfrac{1}{2} n^3 r_{33} E(0) \tag{1.3.12}$$

and thus the index of refraction scales linearly with the applied DC field. Here r_{33} is the principal nonlinear optical coefficient in the electro-optic tensor that defines how the refractive index is modified with an applied electric field.

1.4 Overview

This thesis will present the development of nanofabrication platforms for patterning ISAM films. Chapter 2 will review the technology of poled polymers, Langmuir-Blodgett films, and covalent self-assembly as routes to produce organic nonlinear optical films. Chapter 3 will then focus on ionically self-assembled monolayers which are at the root of this thesis. This review focuses on their potential applications, their nonlinear nature, and on already reported approaches employed to pattern them. Chapter 4 will describe the materials and methods used to deposit ISAM films and to characterize their topography and thermal stability. Chapter 5 will present the development of a fabrication technique used to pattern ISAM films through reactive ion etching and electron beam lithography. Chapter 6 will focus on using a "softer" approach to such patterning by leveraging nanoimprint lithography for such patterning. Chapter 7 will present conclusions as well as future directions of this research.

Chapter 2

Organic Thin Film Deposition

Multiple techniques have been employed to synthesize organic thin films. Organic thin films featuring NLO effects could replace inorganic crystals and result in cheaper fabrication and increased integration capabilities [9]. This chapter will discuss poled polymers, Langmuir-Blodgett films, and covalent self-assembly as three techniques commonly used for such synthesis.

2.1 Poled Polymers

Poled polymers consist of host polymer material with a desired refractive index that is doped with NLO chromophore guests [10]. The doped polymers are dipped or spun onto a substrate but are not nonlinear optically active as-deposited due to the random alignment their chromophores. To impart such polar order, the polymer is heated above its glass temperature while an electric field is applied, allowing the chromophores more mobility to align with the field [11]. This poling process can take from a few minutes to several hours after which the material is cooled back below its glass transition temperature. The electric field is still applied as the temperature is reduced in order to "freeze" in the chromophore alignment. This poling induces the noncentrosymmetry necessary for NLO activity (Figure 2.1) [9,11] and has resulted in r_{33} coefficient of 202 pm/V [11].

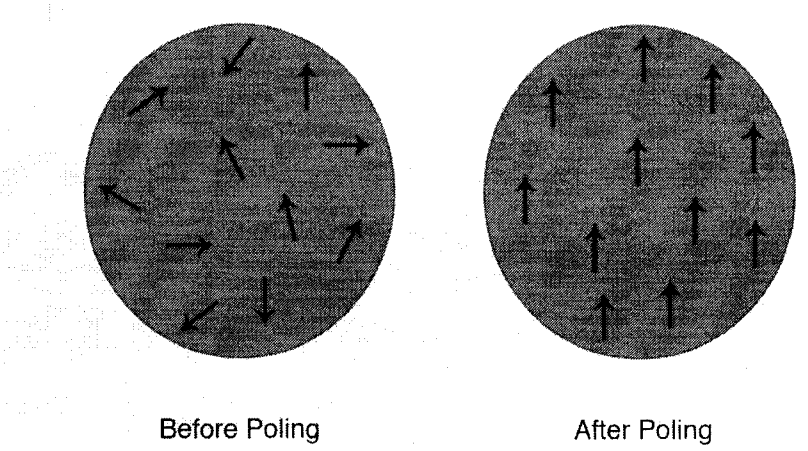

Figure 2.1: Chromophore alignment before and after poling.

Poled polymers are quick and straightforward to deposit with the poling process usually being the most time-consuming [11]. Unfortunately, the chromophore alignment is not perfectly stable [11,12] and relaxes even at room temperature

[9]. This polar stability decreases rapidly as chromophores gain mobility with an increase of temperature, which is impractical for photonic applications exposed to elevated temperature environments [10,13,14]. Introduction of chromophores into a polymer will also typically decrease its glass transition temperature [11], which ideally should be as high as possible for the reasons outlined above. In addition, because the polymers are not bound to any molecules, chromophores have been reported to diffuse to the surface and evaporate or sublimate at higher temperatures [11]. The resulting non-uniform distribution can result in increased scattering of guided light [11].

Covalently bonding the chromophores to the backbone of the polymer has been shown to reduce the decay of chromophore alignment [9] because chromophores have less freedom to move [11]. Covalently bonding a disperse red dye chromophore has also resulted in a second order susceptibility stable at a temperature of 1000 °C at 80-90% of its max value [11]. Nonlinear optical polyesters with chromophores bound to their main chains showed no decay in their second harmonic generation signal after 4.5 days at temperatures as high as 200°C [11]. Cross-linking the polymers after poling has also been demonstrated for locking in the chromophore alignment [9,15], resulting in films showing no decay after 500 h at room temperature [9]. An increased stability has also been realized by increasing the glass transition temperature of the poled polymers through fractionation [15], a process where the polymer is separated by

molar mass. A higher average molar mass leads to an increase in the glass transition temperature.

Patterning poled polymer films based on modification or alignment of the chromophores has been demonstrated. Surface Bragg gratings were patterned into poled polymers through photoisomerization using polarized laser light [16,17]. Similarly, photobleaching with UV light and a photomask resulted in a waveguide and microring structure being patterned into the surface [18]. Nonlinear optical activity was realized by poling before or after surface patterning [18]. Patterned electrode structures also result in areas of aligned and misaligned chromophores [19,20] that have been used to induce birefringence effects [20]. In addition, patterning based on the polymer nature of poled polymers has been reported via reactive ion etching to create a band rejection filter [21], a Mach-Zehnder interferometer [22], and a digital optical switch with rib waveguides [23].

Photonic crystals have been realized in poled polymers using nanoimprint lithography [12,24]. Simultaneously imprinting and poling the materials has also resulted in the creation of NLO gratings [25].

Electron beam lithography has been employed to pattern poled polymers [12, 21]. Upon exposure to the electron beam, poled polymers lost their chromophore alignment due to the depolymerization of the PMMA chain. Development of the exposed areas provides a straightforward method of patterning these films.

2.2 Langmuir-Blodgett Films

Langmuir-Blodgett (LB) films are synthesized using a layer-by-layer film deposition technique relying on hydrophilic and hydrophobic interactions [10]. This technique represents an alternative method to create NLO thin films because of the chromophore alignment inherent to the LB process [26]. Insoluble materials with one hydrophobic and one hydrophilic end are spread across a water surface [27-29]. A pressure is applied to this insoluble material so it becomes close packed and orients its hydrophilic end with the water surface [30]. Substrates are then immersed in this solution. A hydrophobic substrate will deposit a monolayer upon immersion and again on removal (Figure 2.2) [27].

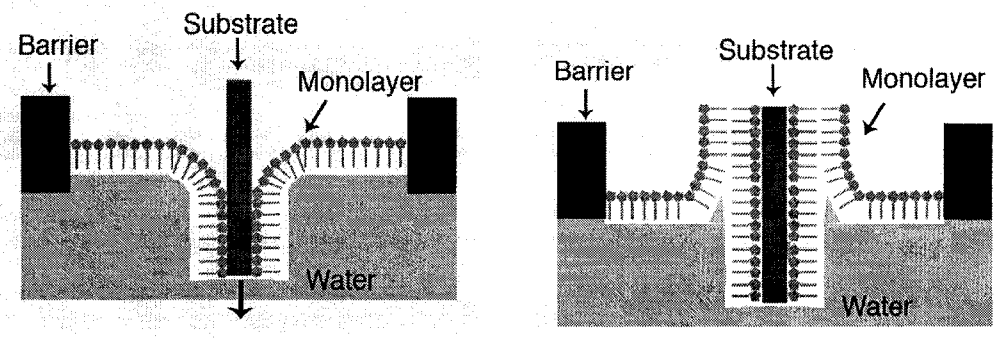

Figure 2.2: Langmuir-Blodgett deposition technique. Monolayer formation occurs upon immersion and again upon removal.

While high electro-optic coefficients have been realized with this technique, LB films still display undesirable attributes. The deposition process is lengthy [10,26], expensive [26], and special equipment [29,31] is needed to control the surface pressure [26,32]. If the condensed material aggregates before deposition, this defect will transfer to the substrate, [29] and any defects that occur in the film persist throughout deposition [31,33,34]. These LB films also possess poor

temporal and thermal stability [13,31,32,34,35]. Increased stability has however been demonstrated with cadmium arachidate by controlling the phase of the deposited monolayer [34]. Another limiting factor is the narrow range of materials can be deposited with the LB technique since such materials must be able to form a monolayer on the surface [32,35].

Langmuir-Blodgett films have been patterned using pulsed laser ablation [28] and scanning tunneling microscopy [36]. Stripe patterns have been observed forming on LB dipped substrates simply by reducing the pressure at which the surface monolayer is maintained [37,38]. LB films that cross-link when exposed to deep UV or electron beam lithography have also been successfully patterned [39]. Microstamping has also been achieved by growing a LB film on a PDMS template [40].

2.3 Covalent Self-Assembled Monolayers

Covalent self-assembled monolayer (CSAM) films possess more stability [41] due to their covalent bonding mechanism when compared to the van der Waals bonding employed in LB films. A monolayer is spontaneously formed on a substrate and then chemically activated so another monolayer can covalently attach to it [10,42,43]. Nonlinear coefficients of 200 pm/V have been realized [43].

The deposition process is lengthy [13,33,44], involving time consuming activation steps needed for the deposition [33]. To prevent defects, the films need 100% reaction yield, so it is difficult to get thick uniform films [31,33]. Defects that do occur will replicate themselves throughout the films. Finally, films formed at high temperatures [13] may not be suitable for integration with IC technology.

Covalent self-assembled monolayer films have been patterned by multiple methods including microcontact printing [45-47], atomic force microscopy [48], scanning tunneling microscopy [48], and electron beam lithography [49].

2.4 Summary

This chapter examined three different methods for the synthesis of organic thin films. A fourth option, ionically self-assembled monolayer films addresses issues such as complicated equipment, long monolayer formation time, stability, and the need for poling, as will be discussed in Chapter 3.

Chapter 3

Ionically Self-Assembled Monolayers

Ionically self-assembled monolayer (ISAM) films are simply synthesized and inexpensive to create. This technique consists of alternatively dipping a charged substrate into oppositely charged polyelectrolytes. This chapter will review the ISAM films' inherent traits, nonlinear optical origin, applications, and the state of the literature related to their patterning.

3.1 Inherent Traits

ISAM films involve a simple growth process based on electrostatic attraction. The strength of these electrostatic bonds results in mechanically and thermally stable organic thin films that maintain their chromophore alignment without the need for poling [2,10,50,51]. Because there are no covalent bonds involved, the polymer chains can shift into their most stable configuration [52]. Deposition occurs at room temperature without the need of complicated deposition apparatus to maintain pressures. Quite often, if only a small number of bilayers are needed, the deposition can also be done manually.

Multiple polyelectrolytes or particles can be incorporated into these nanostructured thin films as long as they posses the charge necessary to sustain the ISAM process [10,26,51,53]. Therefore ISAM films can be designed to display specific properties through such incorporation of suitable materials. The only limitation is that the substrate must be able to posses a surface charge. Versatile materials with various shapes can therefore be employed [2,26,54] [50,55].

This deposition technique is a commercially viable method of creating organic thin films. The process is easily scalable with no limitation on substrate size. In addition, the dipping process can be automated without the need of complex and expensive equipment like those used in Langmuir-Blodgett films [2,56]. Unlike the hour or days it can take to fabricate a monolayer during covalent self-assembly or

LB deposition [13,26,33,44], ISAM films take minutes per bilayer [1,10] with no intermediate chemical activation steps. Finally, unlike LB and CSAM films, [33,34], defects in the film do not propagate throughout the deposition due to the ability of ISAM films to self-heal [57,58]. ISAM films grow over the defects that are introduced during deposition whereas LB and CSAM films will not grow properly over defect sites.

The ISAM deposition process is based on alternately reversing the surface charge of the substrate with each successive layer assembly. Negatively charged sites on a substrate electrostatically bind with the positive charges along the polycation backbone. Because there is a surplus of charged sites on the polyelectrolyte with respect to the substrate, these extra sites repel away from the substrate and push themselves towards the air-film interface. This results in a reversal of the surface charge necessary for the deposition of the next monolayer [59, 60]. This process is repeated when the substrate is dipped into the polyanion solution, resulting in another surface charge reversal (Figure 3.1). These excess charge sites also further repel the deposition of additional layers of the polyelectrolytes. The process is therefore is self-limiting [2,52].

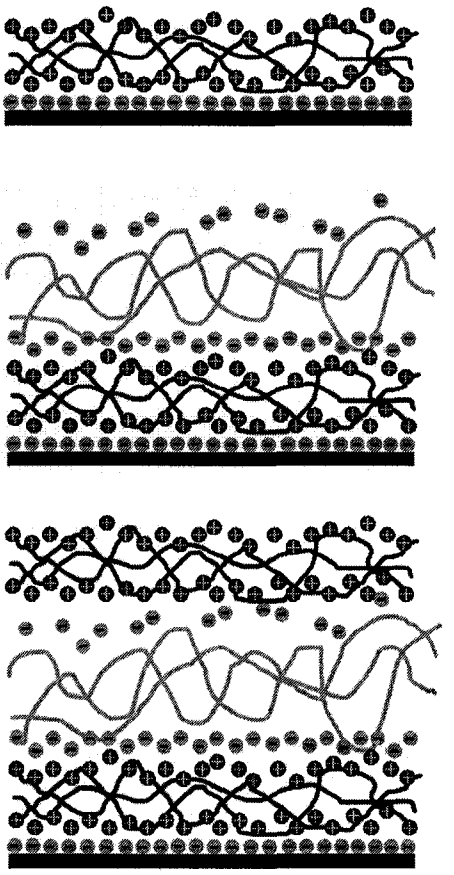

Figure 3.1: Ionically self-assembled monolayer deposition technique. A negatively charged substrate is alternatively dipped in polycation and polyanion solutions, electrostatically building up oppositely charged monolayers.

The thickness of these films can be altered by changing the number of charged sites on the polymer backbone. This is achieved by varying the pH of the polyelectrolytes, and results in variations in bilayer thickness ranging between 0.3 to 5 nm [61]. Decreasing the pH in the polycation or increasing the pH of the polyanion introduces ions into the solution that electrostatically screen the charges on the backbone of the polyelectrolytes [53,61,62]. Since there are fewer charged sites and therefore less repulsion, the polymer chain will display a bent

rather than an elongated configuration, thus resulting in the production of thicker films [14,26,59].

Altering the pH and therefore thickness has also enabled the tuning of the effective refractive index of ISAM films. Incorporating a larger percentage of a higher index polyelectrolyte results in a relatively higher effective refractive index, whereas incorporating more lower index material results in a lower effective index [26,63].

3.2 Origin of Nonlinear Optical ISAM Films

Nonlinear optical (NLO) organic thin films have been receiving increased attention for their potential applications as electro-optic modulators, switches, and frequency doublers [10]. Organic thin films are ideal candidates to replace inorganic crystals such as lithium niobate in NLO applications because of their low cost and ease of processing [10].

The NLO-active polyelectrolyte contains chromophores on its sidechains that preferentially absorb light of a certain wavelength, and reflect or transmit light of another wavelength [53]. The incorporation of these chromophores results in a noncentrosymmetric material system that is necessary for second order nonlinearities [1].

The inherent internal electric field that results from the electrostatically bound layers results in a physical alignment of the NLO chromophores [2]. Unlike poled polymers, this chromophore orientation is both thermally and thermodynamically stable [64]. Measurements of the second-order susceptibility have demonstrated stability over a period of 3 years [64]. At higher temperatures, chromophore alignment was maintained in poly S-119/PAH ISAM films [14]. The intensity of second harmonic generation or frequency doubled light was measured as the films were heated. Although at 150°C the intensity of the SHG signal decreased by ~20%, this signal fully reverted to its original value upon cooling. This indicates that high temperatures do not result in a permanent chromophore misalignment. However, it is likely that some of the electrostatic bonds broke at higher temperatures and reformed upon cooling. This feature suggests that these films can operate at higher temperatures with a stable although decreased NLO effect. This stability is necessary for practical device implementation in environments involving variable temperatures over an extended operating lifetime. While the SHG signal did not completely revert when the films were heated to 250°C, this loss of signal can be attributed to a decomposition of the chromophore and not a permanent loss of chromophore alignment. By using chromophores with a higher decomposition temperature, this loss could be eliminated.

PCBS/PAH films exhibit a r_{33} coefficient between 1-2 pm/V, which is significantly less than lithium niobate with a r_{33} coefficient of 32 pm/V. When ISAM films are

deposited, the chromophores are oriented both towards and away from the substrate due to their binding to the previous and following PAH layer [14]. This competitive chromophore alignment results in reduced second order susceptibility [1,14,59,61]. While there are chromophores in the bulk of the films, they posses random orientations so again there is a high degree of cancellation [59,61].

The second order nonlinear optical effect occurs because of (a) a larger number of aligned chromophores aligned either towards or away from the substrate or (b) the chromophores alignment is not at exactly the same angle at both interfaces resulting in an incomplete cancellation of the NLO effect [14,59].This variation in number or angle can be explained by the different environment of the substrate versus the polyelectrolyte solution [59].

While the NLO coefficients can be increased by changing chromophores, a new hybrid covalent/ionic self-assembly method using Procion Brown has shown r_{33} coefficients of 20 pm/V,[1] roughly two-thirds that of lithium niobate [11]. This method is based on the ionic bonding of the polyanion to the substrate, followed by the directional covalent bonding of a monomeric NLO chromophore to the polyanion layer [13,54,61]. This results in high NLO effects as the competitive dipole alignment and random orientation in the bulk of the film is eliminated, resulting in a high degree of chromophore order [13,54,61]. While these NLO coefficients are not as high as those achieved with poled polymers, their inherent

stability makes them an attractive material system. Another method used to increase the NLO effect resulted in an enhanced plasma resonance by altering the geometry of silver nanoparticles [65].

3.3 Applications

Since the ISAM deposition technique was first demonstrated by Decher and coworkers in the early 1990's [66-68], a wide range of ISAM film-driven applications have been reported. Many materials have been incorporated into ISAM films including chromophores [61,54], nanoparticles [33,65], chitosan [55,69], DNA and viruses [69], enzymes [70], and magnetic particles [71] which have led to the development of ISAM films with a variety of properties.

Potential applications of ISAM films include anticorrosion layers [72], ultra hard coatings [33,56], photovoltaic films [73,74], electrochromic films [75], LED devices [52], and piezoelectric films that do not require further poling [76]. ISAM films created with inorganic nanoparticles have also been developed as a means to increase catalyst and sensor activity due to the resulting increased surface area [60]. The deposition of ISAM films on cotton fibers also leads to the application of functional textiles [58].

Nonlinear optical applications have been of particular interest because the incorporation of chromophores into ISAM films results in nonlinear behavior

[1,14,59,61,64]. Electro-optic modulators, switches, and frequency doubling devices could conceivably be created in these films [10].

Controlling the thickness and refractive index of these films has also led to many optical applications. Precise control over the real and imaginary refractive index of the films was demonstrated by varying the ratio of high and low index bilayers contained in ISAM films [51]. Alternatively, ISAM films created with silica nanoparticles have been used has antireflection coatings [77]. The appropriate optical thickness can be deposited by varying the number of bilayers and the effective refractive index can be controlled by varying the packing density of the nanoparticles [77]. This precise control of thickness was also used to create quarter-wavelength stacks on the ends of optical fibers [57].

Another focus of application has been using ISAM films as sensing materials because of the ability to incorporate sensing materials in them. Non-fiber based oxygen [59], iodate [78], glucose oxidase [70], and pH sensors have been reported. Optical fiber based humidity [79,80] sensors and pH sensors with a detection range between 5 and 8 [81] were reported. Nanometer thick ISAM films deposited on long period fiber gratings have resulted in tunable shifts of their resonant frequency due to the induced change of thickness and index of refraction [26]. Long period fiber gratings showed resonant shift after binding of biotin, streptavidin, and antistreptavidin to the films [82].

ISAM films have made an impact on the field of medicine as well. ISAM films have been investigated as a means to modify implanted structures and increase their biocompatibility. Titanium surfaces were modified by incorporating chitosan in the ISAM films and resulted in an increase of cell proliferation and viability [83]. Protein based ISAM films were grown on a biodegradable porous scaffold with promoted osteoblast cell growth [84]. ISAM films have also been investigated as a means of improving drug loading within a drug delivery system, while increasing the drug release time [69]. Biodegradable ISAM films incorporating DNA particles have been reported as a novel method for gene therapy [69].

3.4 Patterning of ISAM Films

Many methods have been developed to pattern ISAM films. One method treats the ISAM like a conventional resist. Certain polyelectrolytes will chemically react when irradiated with UV light, resulting in the formation of covalent bonds between the monolayers [27,55,85,86]. As a result, the solubility of the exposed areas decreases and the unexposed areas then selectively dissolve in the appropriate solvent. For example, diazo-resin/poly(acrylic acid) ISAM films were exposed and 'developed,' resulting in 9 μm wide features. [55]. This method is promising but is limited to materials that will react in such a manner.

Surface relief gratings were successfully patterned in chitosan/poly S-119 ISAM films [87]. After exposure to linearly polarized light, the chromophore physically reoriented, causing birefringence and dichroism in film. Information storage could

be realized in these films and erased thermally or with circularly polarized light [27]. This method is however limited since it only patterns the surface. The gratings realized here only had a 13 nm height difference [87].

Sculptured ISAM films were also grown on a sacrificial patterned template. After film growth, the films are released, resulting in ISAM 'membranes' featuring 3D ripple structure [88].

Biologically active ISAM films containing proteins or polypeptides were patterned using a lift-off technique [89]. Positive photoresist was patterned using optical lithography, and then immersed in a polycation/polyanion solutions to build up the ISAM films. The photoresist and overlying ISAM films were lifted off in an ultrasonic acetone bath resulting in a 20 μm square array [89]. This technique is limited as only patterns that have exposed photoresist edges would be successfully lifted off.

ISAM films were also patterned into released cantilevers to generate chemical or biosensor arrays. Positive photoresist was spun on an oxidized silicon wafer, patterned, and developed to create anchor points for the ISAM film. Next, the beams were exposed into the resist without being developed, and ISAM films were deposited. The substrate was then soaked in developer and acetone to lift off the overlying films and release the substrates, respectively [70]. Once again,

the lift-off process is limited to features that have an exposed edge. It would be difficult to pattern holes into the films for photonic crystal structures.

3.5 Summary

This chapter overviewed the benefits of the ISAM process and presented the origins of the NLO effect in the films. Multiple ISAM applications and ISAM patterning methods were also overviewed. The following chapter will discuss the details of ISAM deposition and characterization techniques employed in this work.

Chapter 4

Synthesis and Characterization of ISAM Films

Ionically self-assembled monolayer (ISAM) films are an attractive material system for fabricating electro-active devices. The polymeric nature of ISAM films simplifies their processing, and their temporal and thermal stability enables applications requiring higher operating temperatures without loss in chromophore alignment. As will be reported in Chapter 6, this thermal stability opens the door for a potential compatibility with nanoimprint lithography. This chapter describes the materials and methods used to synthesize and characterize ISAM films that can be utilized to fabricate photonic structures.

Synthesis of ionically self-assembled monolayer (ISAM) films is based on the successive electrostatic buildup of oppositely charged monolayers. A negatively charged substrate is dipped into an aqueous polycation solution. The polycations electrostatically bind to the negative charged substrate and result in a charge reversal. The now positively charged substrate is then dipped into a polyanion solution, where the polyanions bind to the previously deposited polycation monolayer, reverting back to a negatively-charged surface (Figure 3.1). The process is then repeated until the desired film thickness is achieved. The ionically self-assembled monolayer films reported here were synthesized at Virginia Tech during the author's visit in Dr. J. R. Heflin's laboratory. The synthesis was performed in collaboration with Cemil Durak, who also provided invaluable training on the solution preparation techniques and on the operation of the automated dipping equipment.

4.1 Experimental Details

4.1.1 Materials

Substrates

ISAM films were grown on glass slides (Fisher Scientific), prime silicon wafers (Silicon Valley Microelectronics, Inc.), and silicon-on-insulator (SOI) substrates (Soitec) consisting of a device layer thickness of 150 nm and an oxide layer of 1 μm. A 590 nm or 40 nm thick oxide layer was thermally grown on the silicon or SOI, respectively, using a Minibrute Single Stack oven. This allows working with a starting surface similar to the glass slides typically employed as substrates for

ISAM synthesis. The substrates were then chemically treated in a piranha solution for 15 min, which consisted of a 2:1 solution of H_2SO_4:H_2O_2. The piranha solution removed organic contaminants and simultaneously induced a negative surface charge on the substrate via hydroxylation that was necessary for ISAM film deposition.

Polyelectrolytes

Originally, hybrid ionic/covalent Procion Brown/PAH films (see Section 3.2) were going to be used because of their higher second order susceptibility. However, that process was not suited for the synthesis of films thick enough for our target application. For proof of concept purposes, PCBS/PAH films were rather used to develop the fabrication techniques that could be later applied to thick Procion Brown/PAH ISAM films.

The NLO-active polyanion, poly[1-[4-(3-carboxy-4-hydroxyphenylazo) benzenesulfonamido]-1,2-ethanediyl, sodium salt] or PCBS , was used in conjunction with the NLO-inactive polycation, poly(allylamine hydrochloride) or PAH. Both these polyelectrolytes (Figure 4.1) were purchased from Aldrich and used without implementing any further purification processes. The average molecular weight of PCBS is 369 g/mol and that of PAH is 90 g/mol. Both polyelectrolytes were dissolved in DI water to create 10 mM solutions. The pH of both solutions was adjusted to 7 by adding NaOH and HCl. All solutions' pH was

adjusted to 7 to ensure that the monolayer thickness remained constant as discussed in Section 3.1.

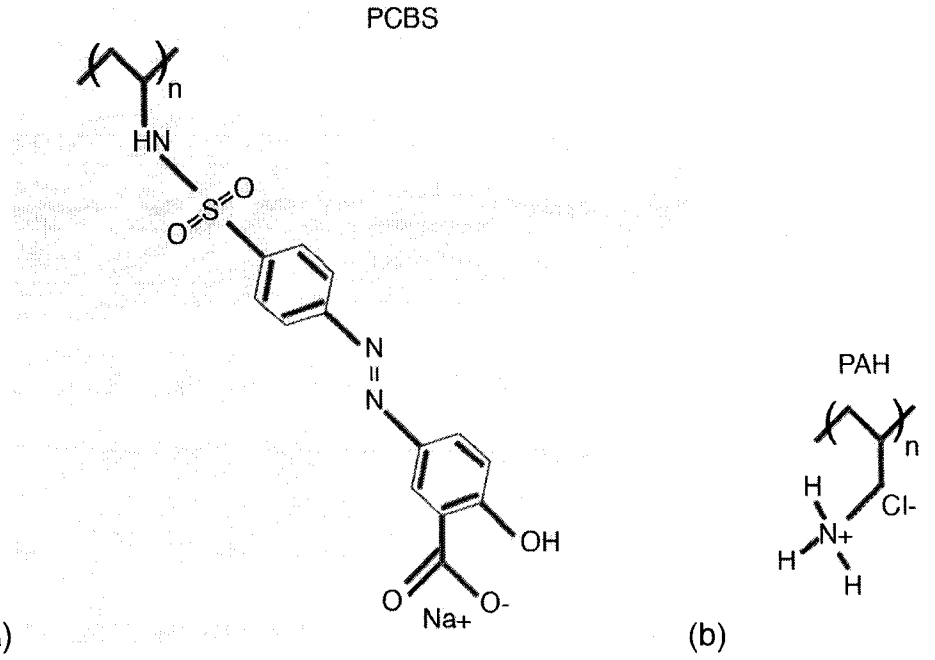

Figure 4.1: Structural formula of (a) the PCBS polyanion and (b) the PAH polycation used to synthesize the ISAM films.

4.1.2 Dipping Process

ISAM deposition can be performed manually, however the film thickness required for our application (>230 bilayers) rendered this approach impractical. Films were synthesized with a Richard-Allen Scientific DS/50 automated slide stainer (Figure 4.2) in Dr. Heflin's lab at Virginia Tech. The dipping process was automated with in-house software and executed at room temperature.

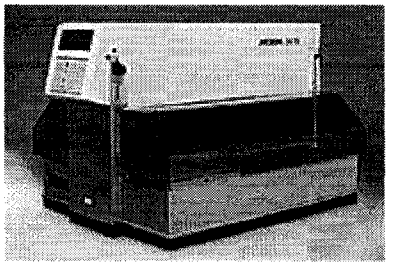

Figure 4.2: Richard-Allen Scientific DS/50 automated slide stainer (www.rallansci.com).

The anionic substrates were dipped in the 10 mM cationic PAH solution for 3 min followed by a DI water rinse for 2 min. The now cationic substrate was dipped in the 10 mM anionic PCBS solution for 3 min, followed by another 2 min DI rinse. To prevent cross contamination of the polyelectrolytes, the DI water was continuously replenished and agitated with an aquarium water pump to remove excess polyelectrolytes that were not ionically bound to the substrate. The solutions were replaced every 12 h. Further optimization of the dipping process could be done in the future to decrease the dipping and rinsing times. PCBS/PAH films have been reported to finish a monolayer deposition in under a minute [61]. Because intermittent drying can affect film properties, films were dried with N_2 only after completion of deposition. The deposition always ended with a PCBS layer to ensure the highest non-linear susceptibility. If the films finished with a PAH layer, some of the chromophores in the PCBS chain are pulled in non-preferential directions [1].

4.1.3 Characterization Equipment

Atomic force microscopy was performed with a DI-3100 Atomic Force Microscope in tapping mode and scanning electron microscopy was performed with a Hitachi S4800 High Resolution Scanning Electron Microscope. Both these

microscopy techniques were used to investigate the topography of synthesized PCBS/PAH ISAM films.

The thermal stability of the PCBS/PAH ISAM films was examined with the Nicolet 8700 FT-IR Spectrometer for Fourier Transform Infrared Spectroscopy (FTIR) and the Kratos Axis 165 X-Ray Photoelectron Spectrometer.

4.2 Characterization

The synthesized PCBS/PAH ISAM films were characterized with specific attention to topography and thermal stability.

4.2.1 Topography

The 500 bilayer PCBS/PAH ISAM films are continuous and homogeneous as shown in Figure 4.3 (a), (b), and (c). However, sites of inhomogeneities are clearly visible in (d) and (e). These inhomogeneous sites may result from agglomeration of polymers adhering to the surface. Another possibility is that contaminants introduced into the polyelectrolytes become incorporated into the film because of ISAM films inherent ability to self-heal [57].

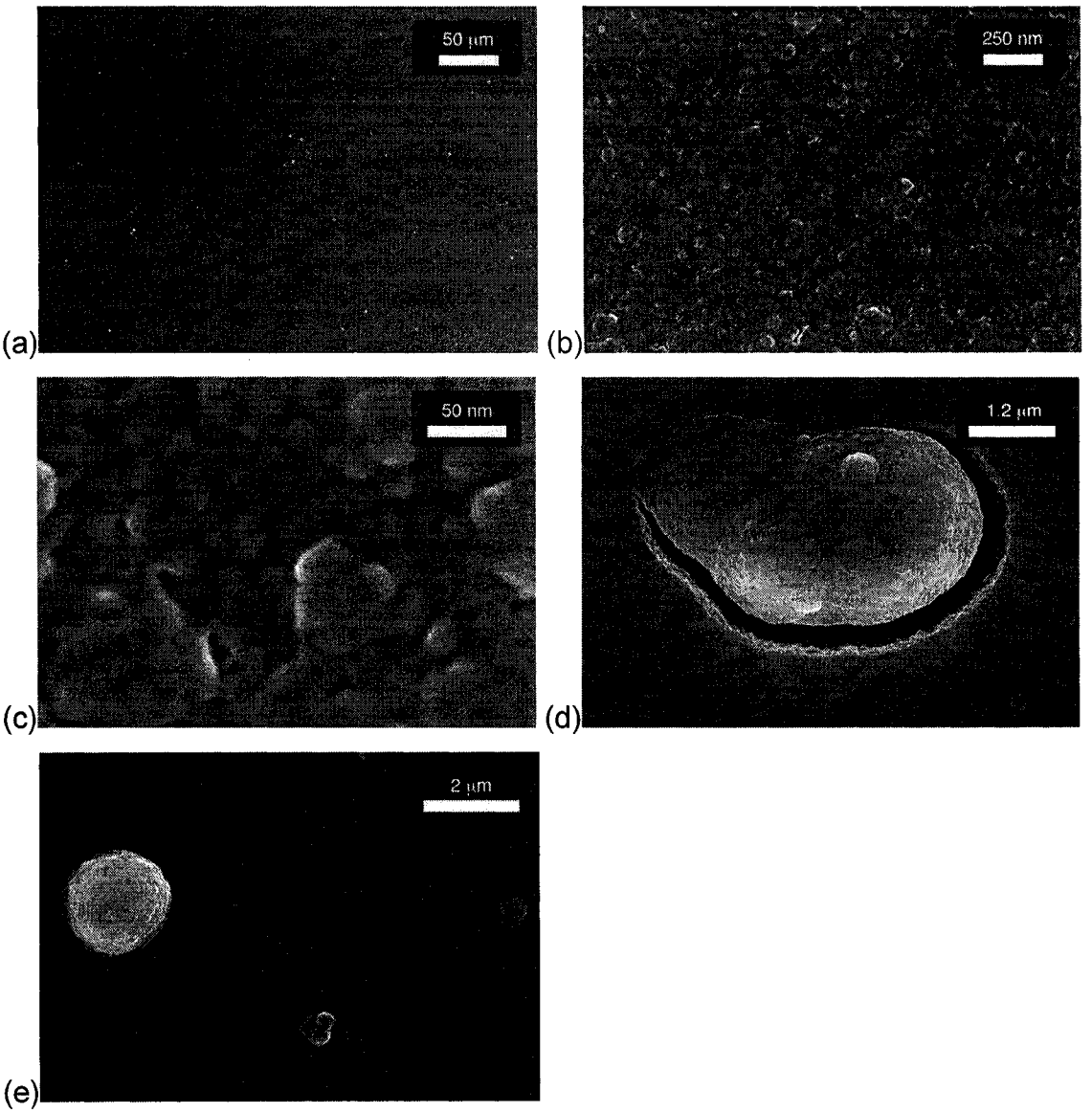

Figure 4.3: SEM images of 500 bilayer PCBS/PAH ISAM films at (a) 300, (b) 60k, and (c) 400k times magnification. Images (d) and (e) show some of the inhomogeneous sites that can be encountered.

Atomic force microscopy images on the 500 bilayer PCBS/PAH films are shown in Figure 4.4. Indicated average roughness of these films was 12.4 nm. Peaks in the films ranged between 80 to 350 nm and can be attributed to the inhomogeneous sites shown in Figure 4.3 (d) and (e).

(a) 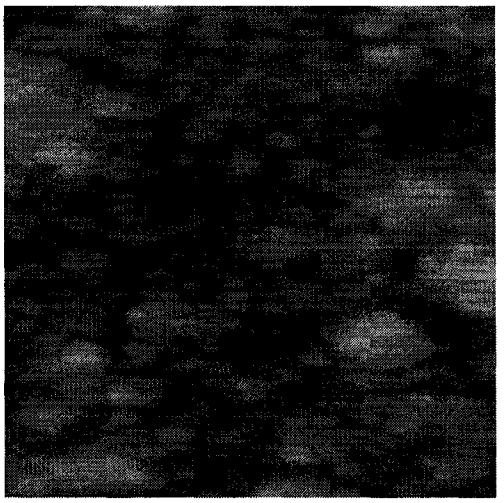 (b) 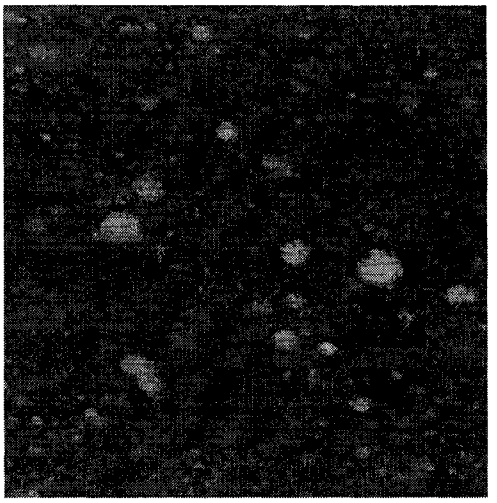

Figure 4.4: AFM images of 500 bilayer PCBS/PAH ISAM film with an (a) 1 μm scan size and a (b) 10 μm scan size.

Inhomogeneous sites are problematic for practical photonic device fabrication. They make uniform resist spinning difficult. Inhomogeneous sites often result in incomplete pattern transfer during imprinting since more time is needed for polymer flow. Since NLO ISAM films are targeted for photonic applications, inhomogeneous sites will scatter the light during guiding, resulting in less-than-optimal power transmission.

The appearance of inhomogeneous sites was reduced by a factor of 40 in 20 bilayer PCBS/PAH films by switching from partially frosted microscope slides to regular slides. The frosting process likely contaminated the unfrosted areas. Using regular slides measurably improved film quality by avoiding that source of contamination.

Filtering the polyelectrolyte solutions was also investigated as a possible means of reducing inhomogeneous sites. Depositing 55 bilayer ISAM films using PCBS/PAH solutions filtered through Whatman polyvinylidene fluoride syringe filters with a pore size of 0.45 μm had no noticeable difference in the quantity of inhomogeneous sites when compared to ISAM films from non-filtered solutions. Therefore, inhomogeneous sites most likely are not a result of contamination of the solutions before deposition, but occur during deposition perhaps because of the presence of particulates or of cross-contamination during dipping.

Further study is necessary to explore other possibilities to reduce these inhomogeneous sites. An obvious option likely to yield positive results is more frequent changing of the dipping solutions. Ultrasonic agitation of the polyelectrolyte baths has been demonstrated as a method to reduce patchy film growth [10] and might contribute to the creation of smoother films.

4.2.2 Thermal Stability

Films fabricated with the ISAM technique have a proven thermal stability. The thermal stability discussed in Section 3.2 combined with the polymeric nature of ISAM films suggested the viability of nanoimprint lithography as a means of patterning these films. However, because different polyelectrolytes were used from those reported in existing studies, the thermal stability of PCBS/PAH films was specifically examined as part of this project.

The thermal stability of the PCBS/PAH ISAM films was analyzed via Fourier transform infrared spectroscopy. The PCBS/PAH ISAM films being tested underwent a 10 m thermal cycle that included heating the films to temperatures up to 200°C and then cooling them back to room temperature. This heating cycle was executed in the Jenoptik HEX 01 hot embossing system and is indicative of temperature changes ISAM films would experience during nanoimprinting.

The same characteristic FTIR spectra, illustrated in Figure 4.5, demonstrate that the bonding within the ISAM films was maintained despite being heated. Of particular interest, the open chain azo (-N=N-) spectra [90] indicative of PCBS can be seen centered around 1600 cm^{-1} and the (C-H) bending indicative of PAH can be seen at 1383 cm^{-1} [91].

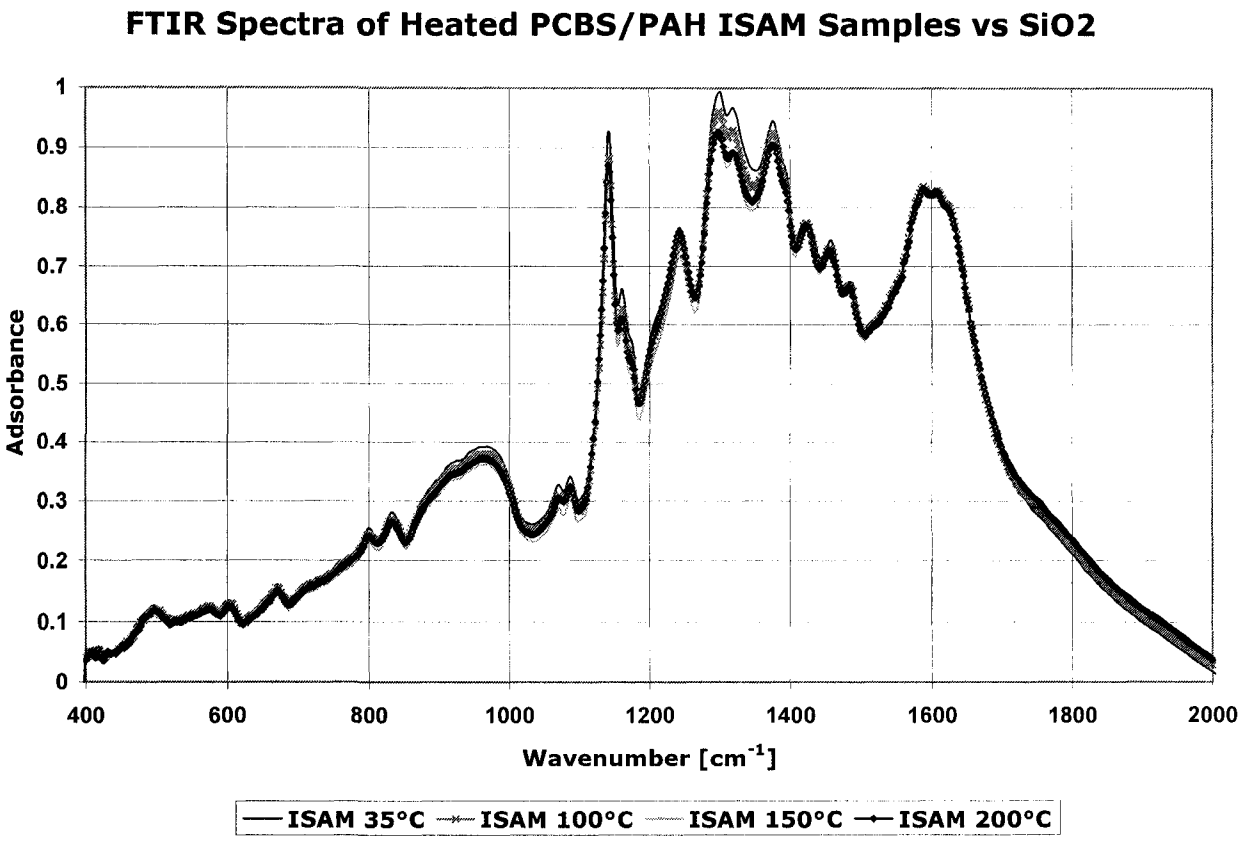

Figure 4.5: FTIR spectra of PCBS/PAH films that have been heated and then cooled back room temperature.

X-ray photoelectron spectrometry (XPS) provided information on how the composition of the films was altered after being heated for 10 min in the Jenoptik HEX 01 hot embossing instrument used in Chapter 6 to imprint these films. The chemical compositions after this heat treatment are reported in Table 4.1. The composition of the PCBS/PAH ISAM films remained constant after being exposed to different heating cycles. The slight fluctuations that do exist in the data can be attributed to small variations in the film morphology due to inhomogeneous sites. These measurements were taken after cooling to indicate

ISAM films' stability after being heated and cooled during nanoimprint lithography.

In order to maximize the second order susceptibility, the final monolayer deposited in the ISAM process was always the NLO-active layer [1]. Hence, because XPS is a surface characterization technique, PBCS should be detected. The XPS data indicates the films are composed of about 21% oxygen, which agrees with the theoretical 21.7% composition of oxygen in PCBS. The carbon composition was found to be around 61% which was significantly higher than the 48.8% theoretically expected. This can be attributed to both surface contamination and the "fuzzy" nature of ISAM films [31]. Therefore, some of the carbon detected can be attributed to contributions from the underlying PAH monolayer because of interpenetration. To test whether contamination or interpenetration increases the carbon content, a further XPS test of a single monolayer of PCBS electrostatically bound to a positively charged substrate would provide the baseline carbon signal.

Table 4.1: Percent mass concentration of PCBS/PAH ISAM films after being heated to different temperatures and cooled back to room temperature.

Temperature	Oxygen	Nitrogen	Carbon	Sulfur
35 °C	20.6 %	12.8 %	60.0 %	6.5 %
100 °C	19.9 %	13.1 %	60.5 %	6.5 %
150 °C	22.0 %	10.2 %	62.2 %	5.5 %
200 °C	21.3 %	11.3 %	61.7 %	5.7 %

4.3 Summary

This chapter described the materials and dipping parameters utilized to synthesize PCBS/PAH ISAM films. Topographical data indicated that the ISAM films possess inhomogeneous sites that need to be removed for practical device fabrication. Thermal characterization shows that the PCBS/PAH ISAM films maintain their composition and bonding, and are thus suitable for nanoimprint lithography. The following chapters present the fabrication of photonic structures in these ISAM films.

Chapter 5

Lithography-Based Fabrication of ISAM Films

While the synthesis and characterization of ISAM films have been the object of considerable attention over last several years, techniques that would allow their cost-efficient and reliable patterning still need to be developed. This chapter reports the development of a fabrication platform for the patterning of PCBS/PAH ISAM films based both on optical and electron beam lithography.

5.1 Experimental Details

The fabrication of ISAM devices has been developed in three stages: i) patterning of a polymer material, ii) patterning of ISAM films, and iii) development of hybrid ISAM/Si photonic structures. Because of the overlap of materials and processes used at each of these stages, these are first described in detail before the fabrication platforms are described themselves.

5.1.1 Materials

Chemicals

Table 5.1 provides an overview of the materials employed, their manufacturers, and their uses.

Table 5.1: Chemicals used in patterning ISAM films with lithography.

Material	Manufacturer	Use
PMMA 950k A2	MicroChem	EBL resist
HPR 504	Fujifilm	Optical lithography resist, polymer representative material, or protective layer
Microposit 354 Developer	Shipley	HPR 504 developer
MIBK:IPA 1:3	MicroChem	EBL developer
Chrome Etch; Semi Grade	FujiFilm	Wet etch
Ethyl Lactate	MicroChem	HPR 504 thinner
Acetone	J.T. Baker	General solvent
Isopropyl Alcohol	J.T. Baker	General solvent
Sulfuric Acid	J.T. Baker	Piranha component
Hydrogen Peroxide	J.T. Baker	Piranha component

Substrates

The substrates used to develop a polymer etching technique were prime silicon wafers (Silicon Valley Microelectronics, Inc.) that were cleaned for 15 min in a

piranha solution consisting of a 2:1 solution of H_2SO_4:H_2O_2. The cleaned substrates then underwent wet oxidation in a Minibrute Single Stack oven at 1000°C for 2 h. This resulted in a 590 nm thick oxide layer, providing an equivalent substrate to the silicon substrates used in ISAM synthesis. ISAM film substrate synthesis is described in Section 4.2.1.

5.1.2 Fabrication Details

Photoresist Spinning

HPR 504 was used both as a positive optical lithography resist as well as a stand-in for the ISAM film itself as the fabrication techniques were being optimized. Such an approach minimized the costs that would have been associated with using the ISAM themselves in the early stages of this development. Spin parameters consisted of a spread cycle for 5 s at 500 rpm and a spin cycle for 30 s at 4000 rpm. The substrates were then soft-baked at 115°C for 90 s to drive off any residual solvents resulting in a thickness of 1.4 μm. After a 1.9 s exposure at 400 nm with an ABM Contact Mask Aligner, the resist was developed for 19 s in 354 developer, rinsed in DI water, and dried with nitrogen.

Polymethyl methacryate (PMMA) of 950k molecular weight dissolved in anisole was used as positive resist for the purpose of electron beam lithography (EBL). Spin parameters consisted of a spread cycle for 5 s at 100 rpm and a spin cycle for 30 s at 4000 rpm. The substrates were then baked at 180°C . This process resulted in a PMMA thickness of 120 nm. Typical Raith 150 EBL exposure

parameters were an accelerating voltage of 2 keV, a 10 μm aperture, and a 15 pA beam current. Following exposure, the PMMA was developed in an MIBK:IPA 1:3 solution for 30 s, placed in a IPA stop bath for 15 s, rinsed in DI water for 15 s, and finally dried with nitrogen.

HPR 504: Ethyl Lactate (EL) 5:7, which was used as an ISAM protective layer, was spun with the PMMA parameters to a thickness of 577 nm.

Chrome Sputtering and Etching

Chrome was used as a polymer masking layer during oxygen reactive ion etching. A Lesker Magnetron Sputtering System operating at a pressure of 2.5 mTorr and a gun power of 300 W, deposited a 35 nm thick masking layer. Initially, these films were sputtered at 7.0 mTorr but these films cracked when heated. Lowering the operating pressure decreased the tensile stress in the films [92].

Manual agitation in a chrome etch solution was not sufficient to 'wet' some periodic structures. Air bubbles would form over certain features, preventing the underlying chrome from being etched. Therefore chrome was etched using ultrasonic agitation until completion of etch was clearly visible, typically after immersion for 15 s.

Organic Polymer Etching

The TRION Reactive Ion Etcher (RIE) was used to dry etch the polymer films. The oxygen plasma was lit with an oxygen flow rate of 15 sccm, an RF power of 60 W, and a chamber pressure of 5 mTorr.

Oxide Etching

The oxide layer on the SOI wafer was etched with an STS Reactive Ion Etcher. The oxide was etched with a CF_4 flow of 20 sccm, a CHF_3 flow of 30 sccm, at a pressure of 100 mTorr, and a RF power of 300 W.

Silicon Etching

A deep silicon cryogenic etch was performed on the Oxford ICPRIE. The exposed silicon was etched with a SF_6 flow of 45 sccm, an O_2 flow of 9sccm, a pressure of 7.5 mTorr, an ICP power of 400W, and a RF power of 6 W.

5.1.3 Optical Waveguide Testing Apparatus

A tunable laser (Santec TSL-210V) with a wavelength range between 1510 nm and 1630 nm guided light through a polarization-controlled lensed fiber. Translation of the lensed fiber end was controlled with a piezoelectric stage such that the tip of the fiber was aligned with the fabricated waveguide. An InGaAs photodetector collected the guided light controlled through an in-house LABVIEW

software program. Measurements were taken by Steve Buswell using Dr. Vien Van's optical apparatus at the University of Alberta.

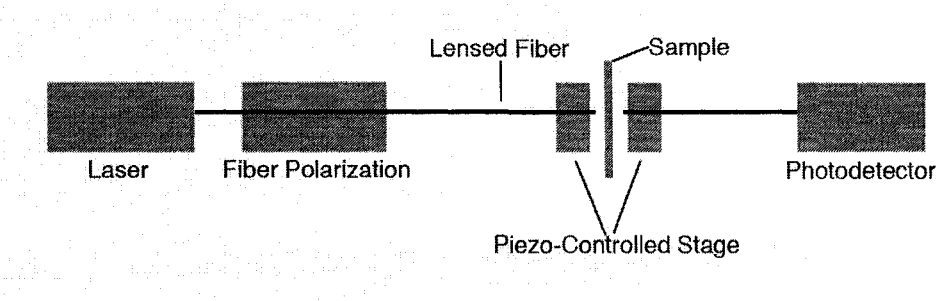

Figure 5.1: Optical test apparatus for guiding light in ISAM waveguides.

5.2 Development of a Polymer Fabrication Process – Phase 1

Fabrication techniques were initially developed in HPR 504 as a proof-of-concept. This enabled multiple fabrication tests to develop a polymer etching method, without destroying ISAM films that involved more time to deposit compared to spinning photoresist.

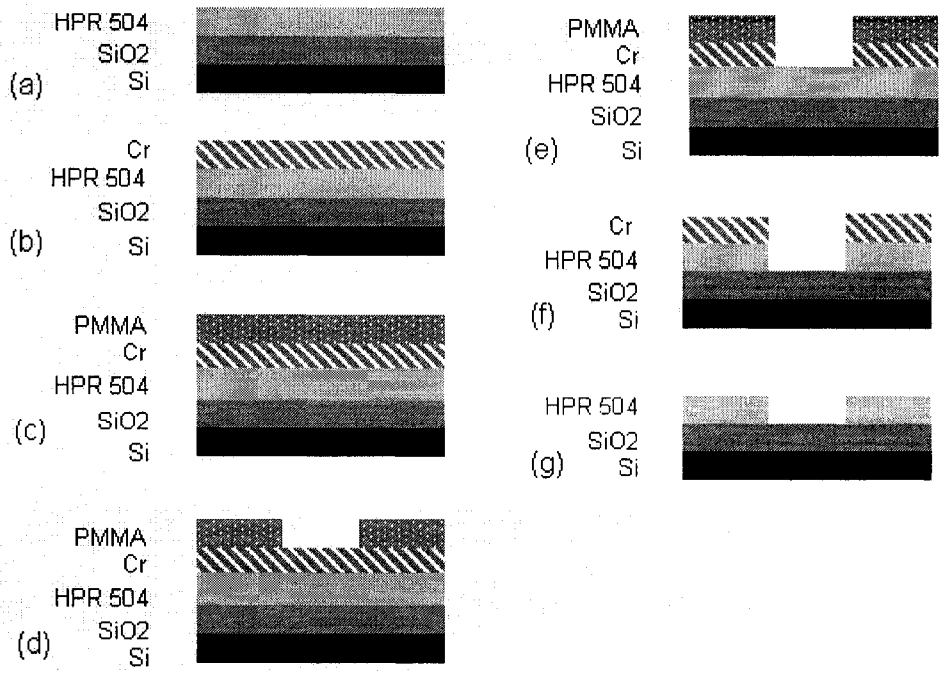

Figure 5.2: Process flow for patterning photonic structures in HPR 504, which was used as an ISAM representative polymer.

Because a standard etch for PCBS/PAH ISAM films is at this point unknown, plasma etching was determined to be the most straightforward method to etch the organic polymers. The process flow for patterning the representative polymeric ISAM material, HPR 504, is illustrated in Figure 5.2. HPR 504 resist is spun on the oxidized silicon substrate in (a). Following resist soft-baking, a low-stress 35 nm chrome masking layer was sputtered onto the HPR 504 in (b). PMMA was then spun and exposed using electron beam lithography in (c) and (d) respectively. After developing the exposed PMMA, the chrome masking layer was etched (e), thereby baring the underlying HPR 504 layer to the oxygen plasma during reactive ion etching (f). The final ultrasonic chrome etch step (g)

results in patterned HPR 504 structures on oxidized silicon substrates. Hexagonal photonic crystal patterns were patterned into the HPR 504 with diameters ranging between 190 and 299 nm as shown in Figure 5.3. Thus, a polymer etching technique was successfully developed.

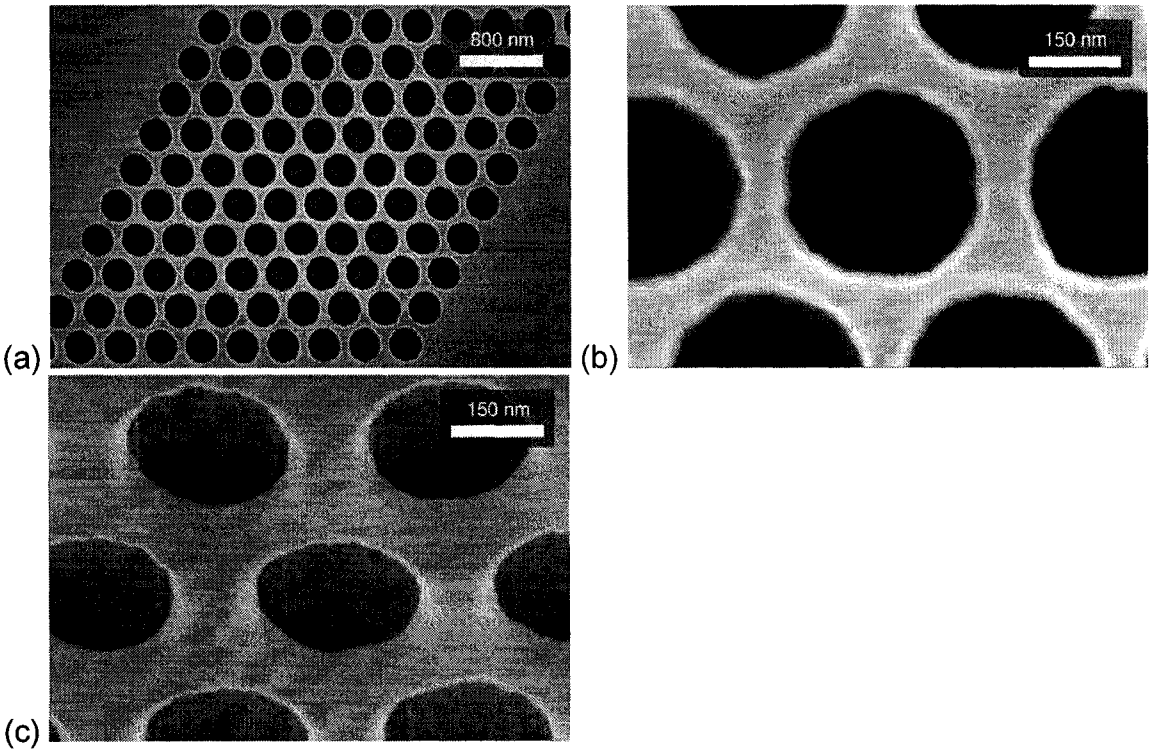

Figure 5.3: Photonic crystal structures were patterned into HPR 504 films using an oxygen plasma.

5.3 Patterning ISAM Films – Phase 2

The organic polymer etching technique developed in Phase 1 was then applied to the etching of PCBS/PAH ISAM films. Initially, optical lithography was utilized because of its relative simplicity compared to electron beam lithography.

It was quickly observed that PCBS/PAH ISAM films were destroyed upon exposure to chrome etch and the 354 developer. Therefore, a layer HPR 504

was then used to protect the exposed ISAM surfaces because of its simple deposition via spinning and its ease of removal in acetone.

In addition, ISAM films tended to crack when the protective HPR 504 resist layer was soft baked. The ISAM films are formed by alternately dipping a charged substrate in oppositely charged aqueous solution and therefore residual water is found in the films. The cracking was attributed to a buildup of pressure of water vapour unable to escape through the overlying HPR 504 protective layer. Before any processing began, the ISAM films were therefore preheated on a hot plate at 180°C for 1 h. Figure 5.4 shows the micrograph of such a crack propagating throughout the ISAM films. From that figure, it is appears that inhomogeneous sites seem to promote cracking. The protective HPR 504 layer was also baked at 180°C for 1 h to drive off any residual solvents. Insufficient baking resulted in the cracking of the protective chrome layer, perhaps again because of pressure buildup as the solvent vapor tried to escape.

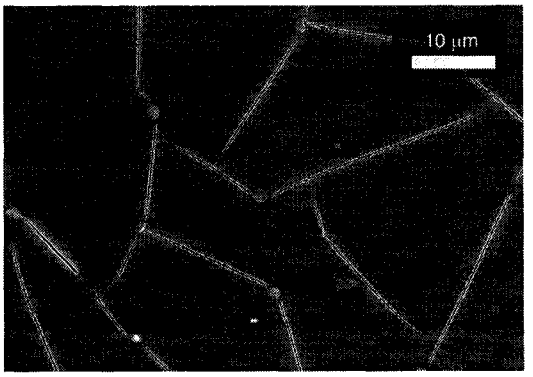

Figure 5.4: Crack formation in ISAM films.

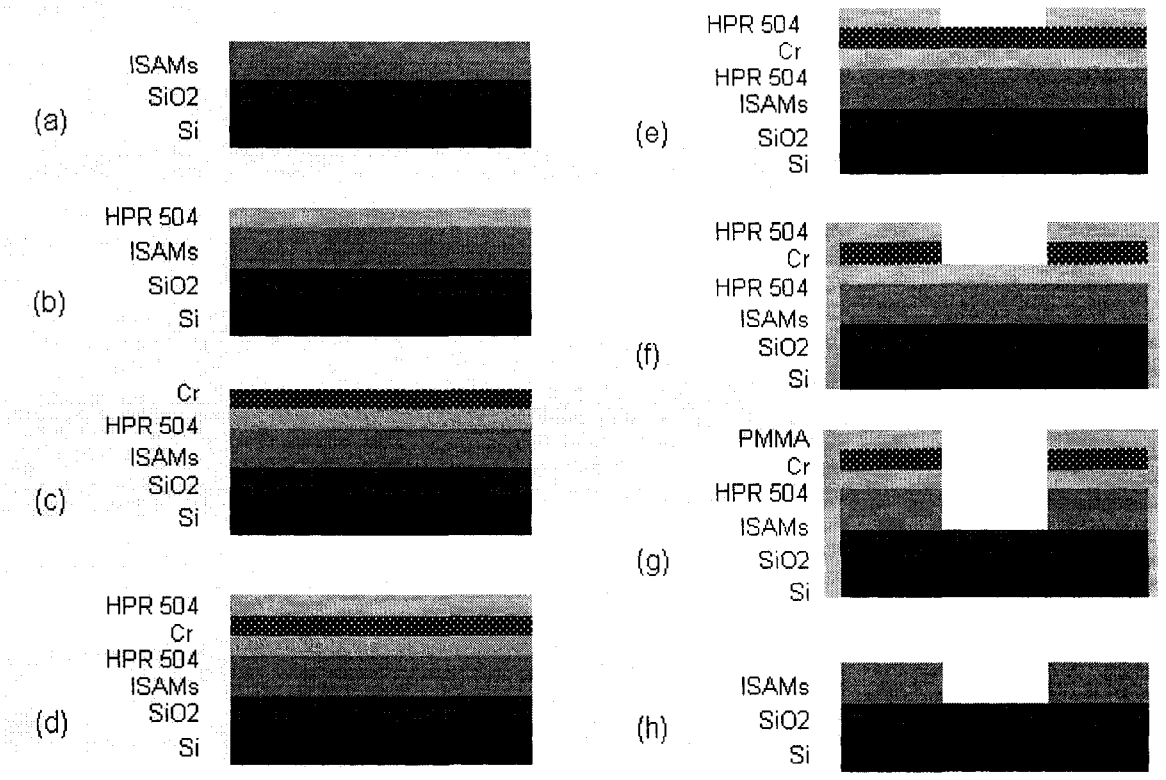

Figure 5.5: Modified ISAM fabrication process flow.

A modified process flow is shown in Figure 5.5. The ISAM films were prebaked (a) to prevent ISAM crack propagation. A protective layer of HPR 504: EL 5:7 was spun on the ISAM films (b) to prevent contact with chrome etch and 354 developer. After baking the protective layer, a 35 nm low stress chrome masking layer was sputtered onto the substrate (c). HPR 504 resist was then spun on the chrome masking layer (d) and patterned using optical lithography (e). The sides of the ISAM films were coated with a protective layer of HPR 504 and then the exposed resist was developed. The chrome masking layer was etched (f), enabling the HPR 504 and underlying PCBS/PAH ISAM layer to be etched by the oxygen RIE plasma in (g). Finally the protective HPR 504 and chrome masking

layers are removed in an ultrasonic acetone bath leaving patterned ISAM films shown in (h).

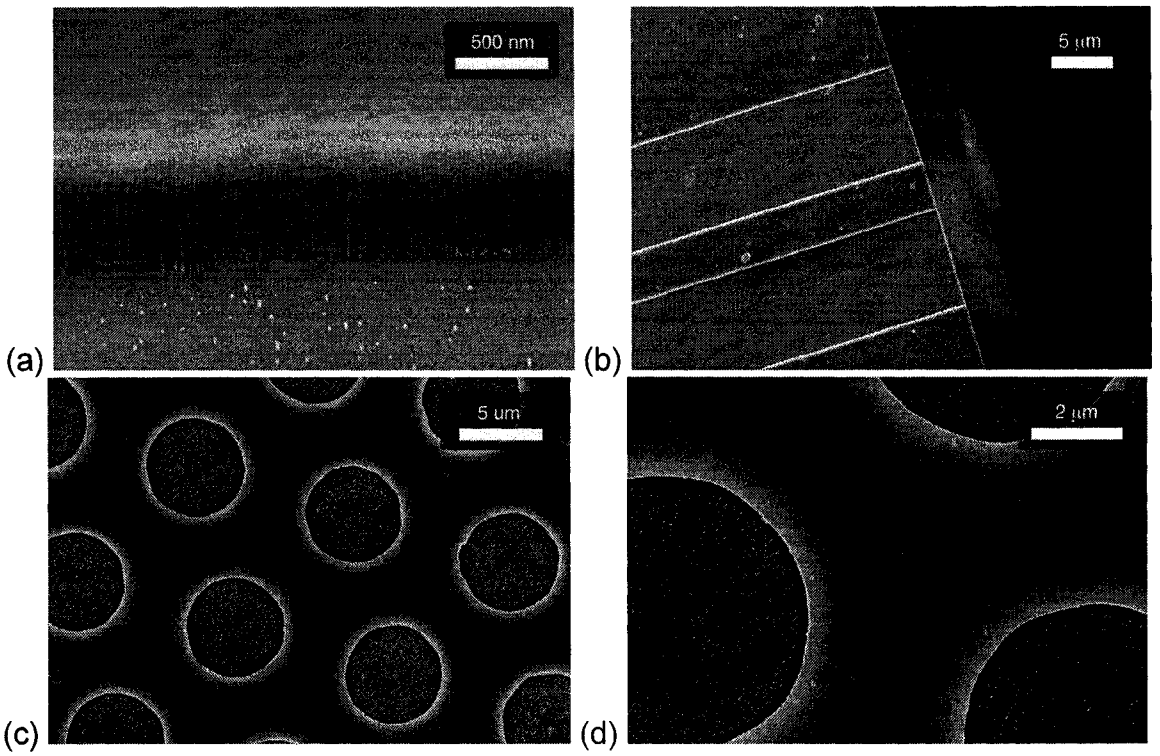

Figure 5.6: PCBS/PAH ISAM films patterned with optical lithography. The sidewall etching profile can be seen in (a). A top-down view of an optical waveguide in (b), and photonic crystal structures are shown in (c) and (d).

Patterned PCBS/PAH ISAM films are shown in Figure 5.6. The oxygen plasma reactive ion etching (RIE) side profile is shown in (a). The RIE successfully etched through both the HPR 504 protective layer (lighter polymer above) and the ISAM films (darker polymer below). The etch is very anisotropic, however the walls are rougher than desirable. This roughness can be attributed to both the raggedness of the etched chrome and the ion bombardment during RIE etching. It has been shown that sidewall roughness can decrease by varying the RF power and oxygen flow rate [93]. By applying these methods and finding a more

suitable chrome etch, this roughness could be significantly decreased. In (b), the diced edge of a 4 μm PCBS/PAH ISAM waveguide with 8 μm cladding on either side is shown, whereas in (c) and (d) images of 5 μm hexagonal photonic crystal structures are shown.

With a fabrication platform now developed for patterning PCBS/PAH ISAM films, electron beam lithography (EBL) was used to pattern the ISAM films. The process flow in Figure 5.5 still applies, however in step (d), PMMA 950k EBL resist was spun on the substrates. After exposure with the Raith 150 EBL system, the substrates were developed, (e) and then a protective HPR 504 layer was applied to the edges. Prior protection was not necessary as the solvents used to develop PMMA do not attack the ISAM films.

Figure 5.7 shows the micrograph of hexagonal photonic crystal structures that were exposed with EBL and subsequently etched into the ISAM films. The chrome masking layer and underlying HPR 504:EL 5:7 layer still remains, and it is evident that the chrome masking layer is quite ragged and transfers into the PCBS/PAH ISAM films. However, photonic crystals with a lattice spacing of 710 nm and circle diameters ranging between 550 nm and 650 nm were successfully patterned with electron beam lithography.

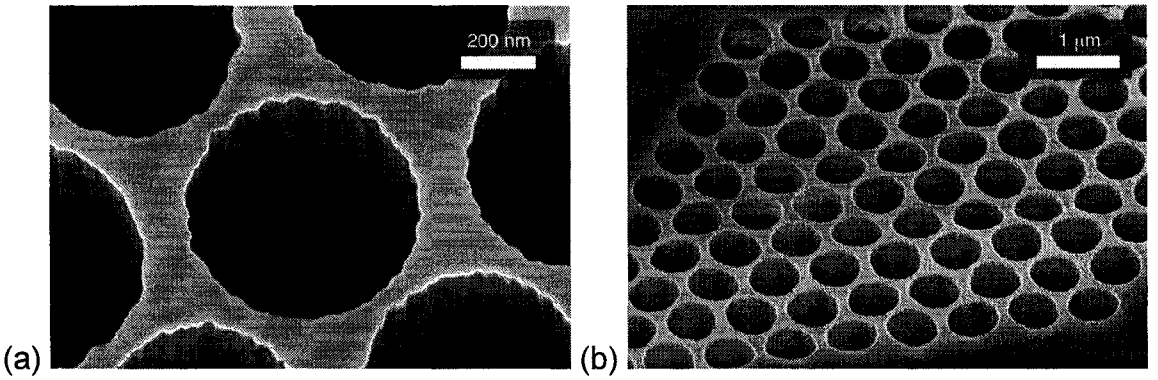

Figure 5.7: Photonic crystal structures fabricated in ISAM films using electron beam lithography.

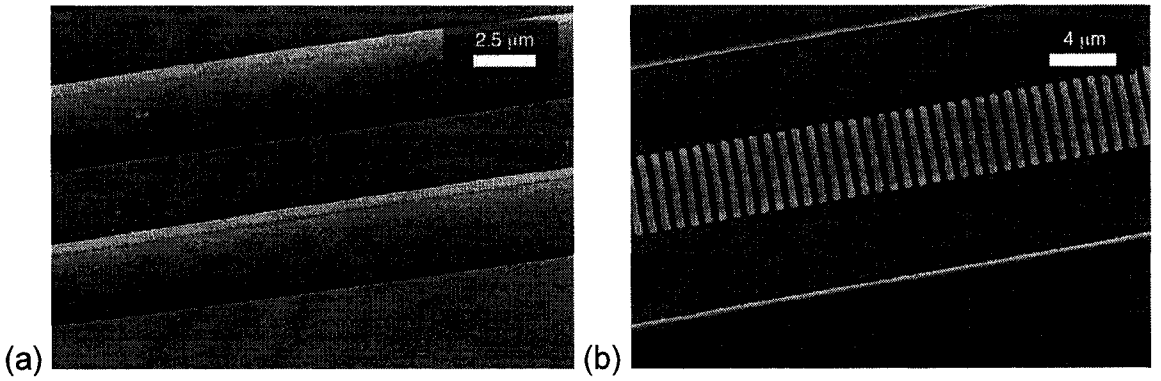

Figure 5.8: Simple waveguides, (a), and Bragg grating containing waveguides, (b) were fabricated in ISAM films.

Simple waveguides and Bragg gratings were also fabricated in 400 bilayer PCBS/PAH ISAM films as shown in Figure 5.8. The waveguides shown in (a) were 3 μm wide with 4 μm cladding on either side. The Bragg gratings waveguides had equivalent dimensions. However, these were patterned with lattice spacing ranging between 560 to 650 nm, specifically in (b) a 570 nm lattice spacing. Because both the Bragg gratings and photonic crystal dimensions are subwavelength, the field sees a homogeneous material.

A laser tuned to 1510 nm did successfully transmit through the waveguide shown in Figure 5.8 (a). From the 10 mW laser source, guided transmission of 240nW was observed. Coupling inefficiency does not completely explain this loss. Transmission measurements of silicon waveguides measured on the same setup was found to have powers 2 to 3 orders of magnitude higher. The sidewall roughness and the inhomogeneous sites found within the PCBS/PAH ISAM films also contribute to this loss, both cases clearly visible in Figure 5.9.

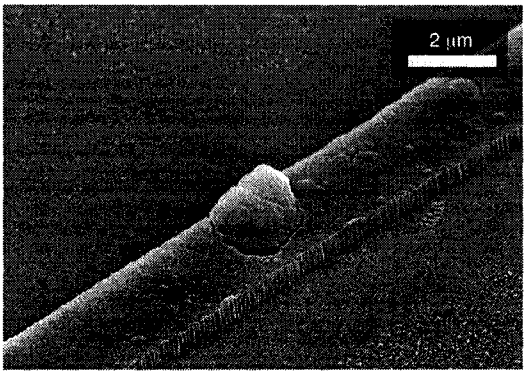

Figure 5.9: PCBS/PAH ISAM films waveguide film with both inhomogeneous sites and sidewall roughness.

5.4 Hybrid ISAM/Si Waveguides – Phase 3

Creation of a novel hybrid ISAM/Si waveguide based on photonic crystals was done in collaboration with Steve Buswell. The hybrid structure was developed so that the photonic bandgap was based on the higher refractive index and stronger guiding ability of silicon. In this sense, light would be guided through the silicon waveguide, while still leveraging the nonlinear optical properties of the ISAM films through the evanescent field. Hybrid ISAM waveguide structures have been

reported previously [10], but for the purpose of decreasing ISAM deposition times and not for increased light confinement.

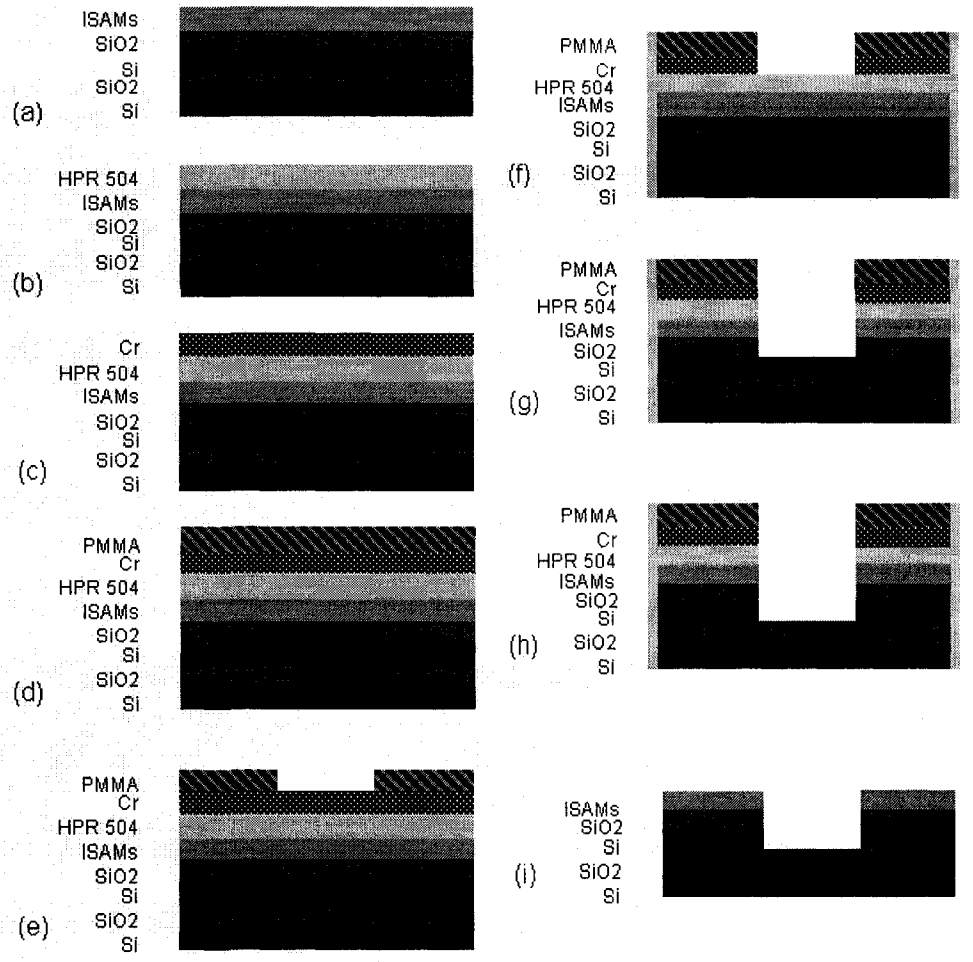

Figure 5.10: Process flow for the hybrid ISAM/Si photonic structures.

The process flow for the hybrid ISAM/Si fabrication process is shown in Figure 5.10. A SOI substrate with a 240 bilayer PCBS/PAH ISAM films was used as the substrate. Steps (a) through (f) were not altered from Phase 2. However, after patterning of the ISAM films, the underlying oxide layer was etched in a reactive ion CF_4/CHF_3 plasma (g), to expose the underlying silicon device layer that was

cryogenically deep silicon etched (h). After the protective HPR 504 and chrome masking layer was removed in an ultrasonic etch, a hybrid ISAM/Si photonic crystal waveguide was produced as shown in Figure 5.11.

A side-view of the hybrid ISAM/SI waveguide is shown in (a), while a photonic crystal waveguide is shown in (b). Light was not successfully guided through these structures in spite of the use of silicon. This is most likely attributed to the sidewall roughness that was transferred into the underlying silicon device layer from the previous ISAM etch as discussed in Section 5.3.

(a) 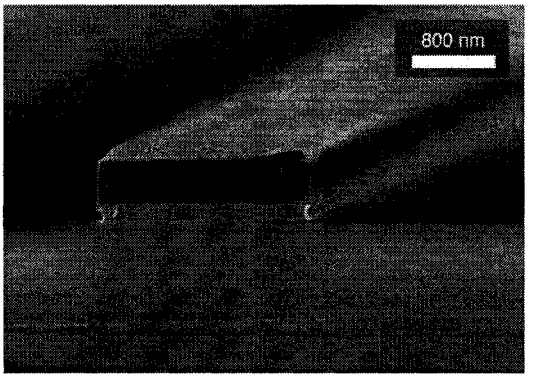

(b) 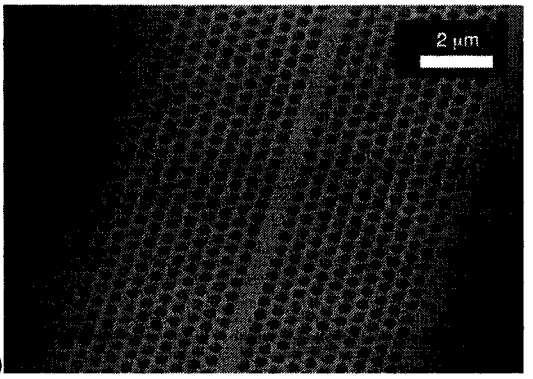

Figure 5.11: Hybrid ISAM/Si photonic crystals were fabricated. Shown is (a) a side-view of the waveguide structure and (b) a photonic crystal waveguide.

5.5 Summary

This chapter detailed the development of a fabrication platform for the patterning of ISAM films. To my knowledge, this is the first time reactive ion etch techniques have been successfully applied to pattern such films. Simple waveguides, Bragg gratings, and photonic crystal structures were all realized in PCBS/PAH ISAM films through the use of an oxygen plasma. Work still needs to be done on

decreasing the sidewall roughness and inhomogeneous sites before practical photonic devices can be created. However, one method that would result in both decreased fabrication time and sidewall roughness is nanoimprint lithography, which is discussed as an alternative patterning technique in the next chapter.

Chapter 6

Nanoimprint Lithography of ISAM Films

Nanoimprint lithography is a commercially viable fabrication method because of its low costs and high throughput. Thermal characterization of ISAM films presented in Section 4.4.3 indicated that PCBS/PAH films are a suitable candidate for NIL. This chapter will detail the use of nanoimprint lithography to fabricate photonic structures in ISAM films.

Nanoimprint lithography (NIL) involves physically deforming a thermoplastic polymer with a mold by applying a constant force above the materials glass transition temperature. Under these conditions, the polymer flows into and conformably contacts the mold. Demolding occurs after the system temperature is lowered, resulting in an irreversible change in the topography of the imprinted polymer that is the negative image of the mold.

6.1 Experimental Details

6.1.1 Materials

Multiple chemicals were used to develop a nanoimprint lithography technique. Table 6.1 provides an overview of the materials, their manufacturers, and their uses.

Table 6.1: Chemicals used in patterning ISAM films with nanoimprint lithography.

Material	**Manufacturer**	**Use**
PMMA 950k A2	MicroChem	EBL resist and representative polymer system
MIBK:IPA 1:3	MicroChem	EBL developer
Chrome Etch; Semi Grade	FujiFilm	Wet etch
Trichloro(1H,1H,2H,2H-perfluorooctyl)-silane	Aldrich	Anti-adhesion layer
Red Hi-Temp Silicone	Permatex	Mold and substrate adhesive
Acetone	J.T. Baker	General solvent
Isopropyl Alcohol	J.T. Baker	Developing stop etch and general solvent
Sulfuric Acid	J.T. Baker	Piranha component
Hydrogen Peroxide	J.T. Baker	Piranha component

Substrates

Substrate preparation has been detailed in previous chapters. Preparation of ISAM substrates and films are described in Section 4.2.1. Silicon substrates and cleaning is described in 5.1.1

6.1.2 Fabrication Details

Photoresist Spinning and Developing

Spinning and developing parameters have been discussed in the previous chapter and details can be found in Section 5.1.2.

Chrome Deposition and Etching

Chrome was evaporated using an electron beam evaporation system to a thickness of 30 nm as measured by a crystal thickness monitor. Sputtering was not used because of step coverage issues. This chrome layer was later removed with a wet chrome etch solution.

Silicon Etching Procedure

Deep silicon etching was performed using two different systems depending, on their respective availability. An STS ICPRIE was used to deep etch silicon at a pressure of 20 mTorr, with a C_4F_8 flow of 80 sccm and a SF_6 flow of 100 sccm. The ICP power was 2.5 kW and the RF power was 20 W. A deep silicon cryogenic etch was also performed on the Oxford ICPRIE. The exposed silicon

was etched with a SF_6 flow of 45 sccm, an O_2 flow of 9 sccm, a pressure of 7.5 mTorr, an ICP power of 400 W, and a RF power of 6 W.

Silanization

To prevent the polymer from adhering to the silicon molds, a monolayer of trichloro(1H,1H,2H,2H-perfluorooctyl)-silane was applied to the Si master as an antistiction layer. The silane and mold were placed under vacuum for 1 h, resulting in a monolayer of silane forming on the mold.

NanoImprint Lithography

The Jenoptik Hex 01 hot embossing system was used to imprint the ISAM films before May 2007, and the Jenoptik HEX 02 hot embossing system was used after that point. The system consists of two horizontal metal plates whose temperature, position, and force exerted are controlled by manufacturer provided software. All NIL was performed under vacuum. Both the PMMA and the ISAM films were imprinted at around 145°C. Forces varied depending on feature size. As the area of the tool increased, the force would also have to increase to maintain the same pressure. Typical forces for nanometer-scale tools were between 1-2 kN and for micron-scale tools were between 5–20 kN.

6.1.3 Optical Characterization

Optical Waveguide Testing Apparatus

The apparatus used for the characterization of nanoimprinted waveguides was the same as the one used in the previous chapter. Description of this system was reported in Section 5.1.3.

Second Harmonic Generation Apparatus

Second harmonic generation (SHG) measurements were performed by Cemil Durak in Dr. J. R. Heflin's lab at Virginia Tech. Second harmonic generation was measured using a Q-switched Nd:YAG pulsed laser (Spectra Physics Quanta-Ray GCR 130) at 1064 nm. The pulse frequency was 10 kHz and the pulse width was 15 ns with an energy of 500 mJ. The beam encountered the first prism, where over 95% of the energy was dumped. The remaining reflected beam was further reduced through energy reduction filters and then polarized. The high pass filter prevented any light with a wavelength above 700 nm from being transmitted, therefore eliminating any SHG produced from previous optical elements. The beam was then split to a photodetector that recorded the reference beam and to a focusing lens that focused the beam onto the sample. The sample was mounted on a stage controlled by stepper-motors. After transmission, the beam was collimated and then transmitted through a band-pass filter (between 380 nm and 600 nm) which removed the 1064 nm component of the beam. The final spike filter, at 532 nm, ensured that the only light collected by the photomultiplier tube was from second harmonic generation.

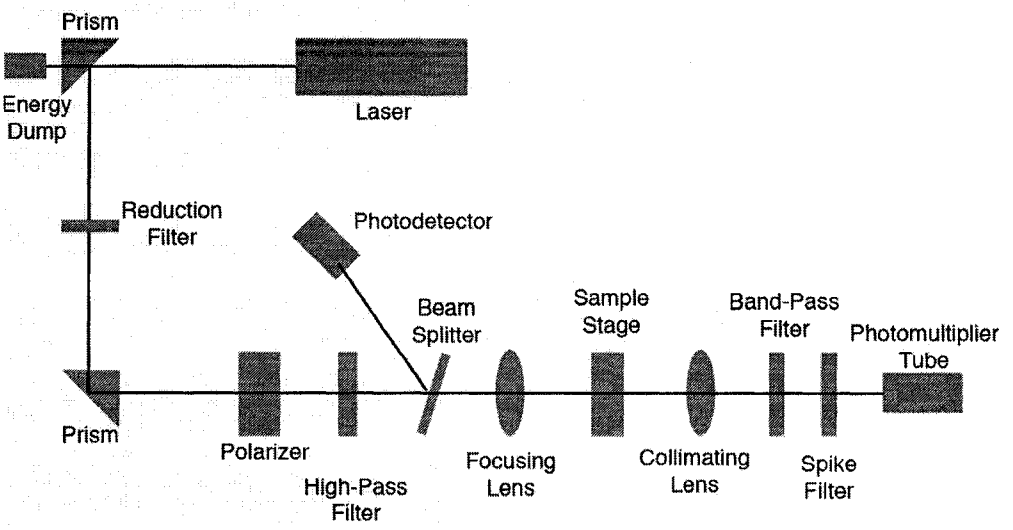

Figure 6.1: Second harmonic generation measurement apparatus.

6.2 Development of Nanoimprint Molds – Phase 1

A suitable mold had to be created before imprinting in ISAM films could be performed. Silicon was used to create the molds because of its ease of processing and access to facilities. While silicon is not as wear-resistant as a nickel mold, it is significantly cheaper and therefore enables more flexibility in terms of design modification.

The process flow for creating these molds is shown in Figure 6.2. Both optical lithography and electron beam lithography were used to create molds in silicon. The appropriate resist was spun on the silicon substrates (a) and exposed (b). A 30 nm thick chrome layer was evaporated onto the patterned substrate (c). Lift off was performed to remove the resist and overlying chrome layer, resulting in a negative-toned chrome patterned in (d). The chrome pattern masked the

underlying silicon during deep silicon etching in (e). The chrome was removed, leaving a silicon mold that was silanized to prevent polymer adhesion in (f).

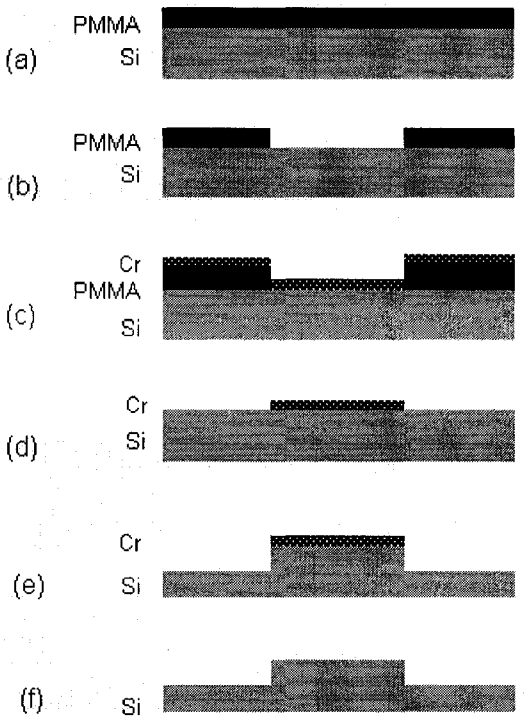

Figure 6.2: Fabrication process for the creation of silicon molds.

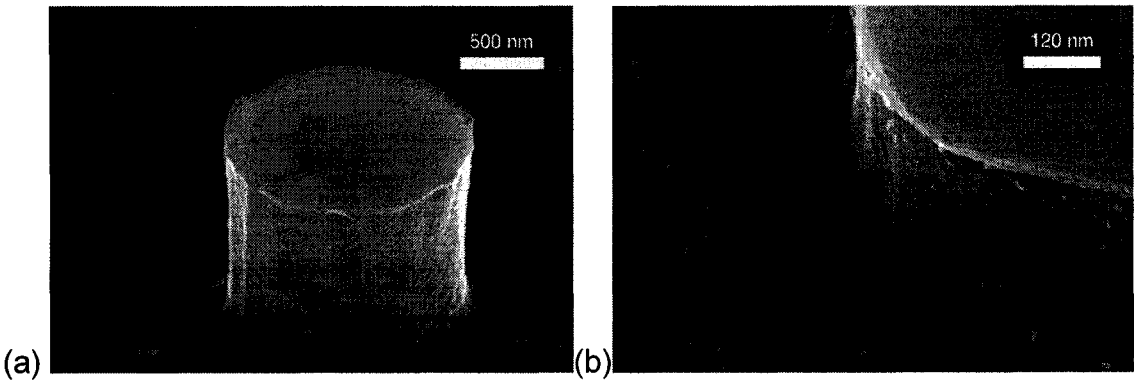

Figure 6.3: Etching profile typical of the deep silicon etching process using (a) the Oxford ICPRIE cryogenic silicon etch and (b) the STS ICPRIE deep silicon etch.

The typical etch profile that results after deep silicon etching are shown in Figure 6.3 for both the Oxford ICPRIE and the STS ICPRIE. Both etches result in an anisotropic etch that is required by NIL. In addition, both etches impart a degree of roughness to the silicon mold. However, the Oxford's silicon etch appear to generate smoother sidewalls but rougher floors than the STS' silicon etch. Molds made from both systems successfully imprinted ISAM films. The smoothness of these molds could be further enhanced by exposing the silicon to a short thermal oxidation step followed by an oxide removal step.

A uniform 1 μm pillar array fabricated using the cryogenic deep silicon etching procedure is shown in Figure 6.4. The etching process resulted in a very uniform array with no apparent underetching.

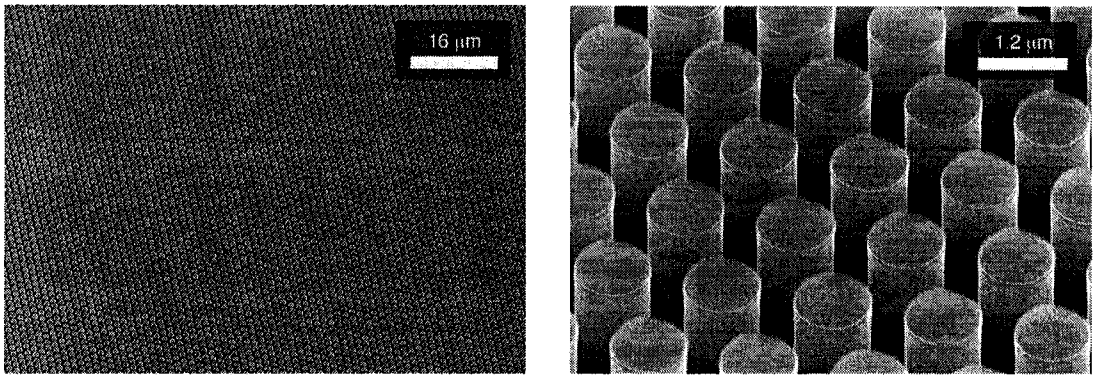

Figure 6.4: An uniform silicon imprinting mold created deep silicon etching process for micron scale imprinting. .

Electron beam lithography was also used to fabricate nanometer-scale pillar arrays as shown in Figure 6.5. In (a), arrays of pillars of various diameters, in (b) 490 nm diameter pillars, and in (c) a 3 μm waveguide with Bragg grating with a period of 590 nm are shown.

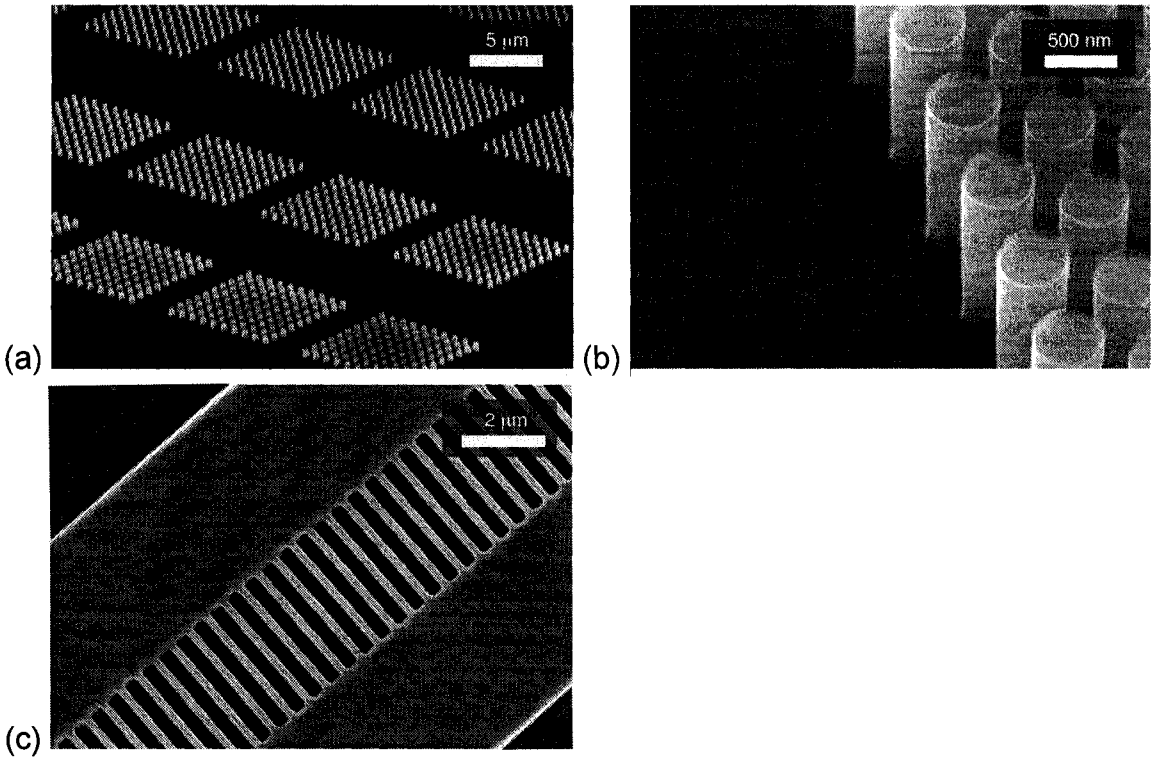

Figure 6.5: Nanoimprint lithography molds created with electron beam lithography.

6.3 NIL in PMMA – Phase 2

Following the fabrication of silicon molds, representative polymer films were imprinted. PMMA 950k was spun onto silicon wafers to a thickness of 500 nm (by multiple spin depositions). PMMA was used as the representative polymer to develop the nanoimprinting process without destroying ISAM films that are more time consuming to make.

Figure 6.6 shows PMMA patterned with (a) an array of 4 μm pillars, (b) 2 μm waveguides, and (c) an array of 460 nm pillars. For these imprints, the mold and polymer were sandwiched between two glass plates during nanoimprinting. This method had been used for previous nanoimprinting work performed and was advantageous because no complicated mounting technique had to be used. Developing the NIL process for PMMA enabled the temperatures to be adjusted so that the top and bottom plates were within 2°C to prevent polymer lip formation and thermal stress in the films.

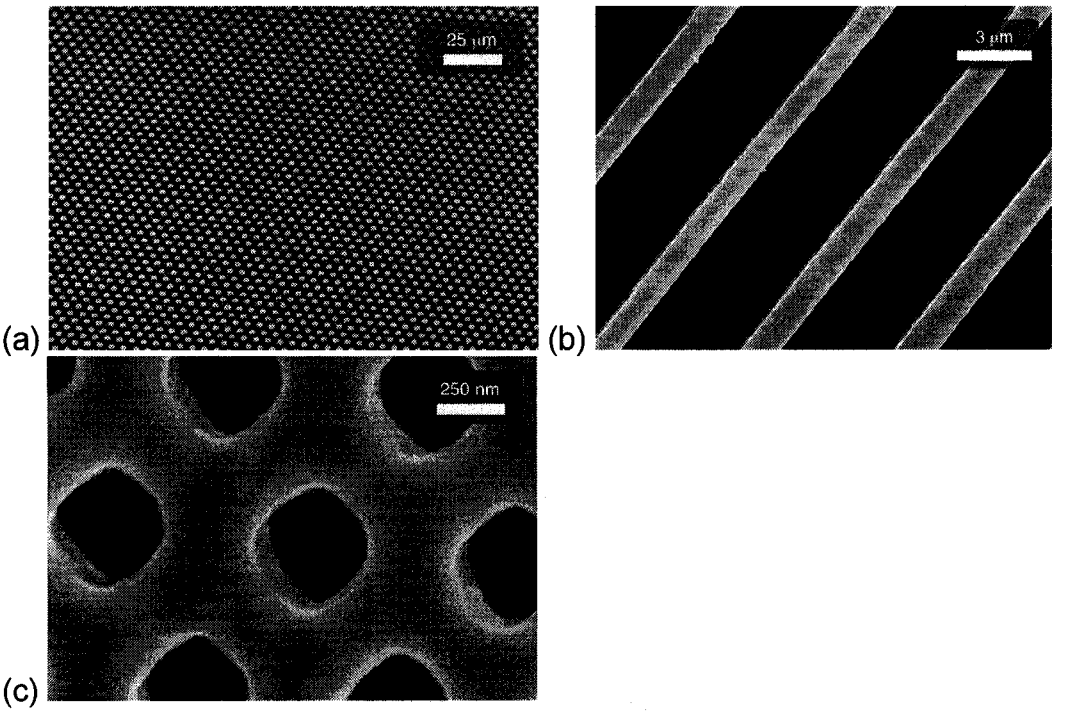

Figure 6.6: PMMA imprinted with a (a) 4 μm diameter circle array and (b) 2 μm waveguides whose silicon mold was created with optical lithography. A 460 nm pillar array, (c) was imprinted using a silicon mold created with electron beam lithography.

6.4 NIL in ISAM Films - Phase 3

Ionically self-assembled monolayer films were chosen as an ideal candidate for nanoimprint lithography because of their polymer nature and thermal stability. The nanoimprinting technique developed in Phase 2 was applied to PCBS/PAH ISAM films.

Figure 6.7 shows micrographs of initial imprinting results achieved in PCBS/PAH films. Micron scale (a) and nanometer scale features were successfully produced in the films. In (a), the mold did not penetrate the film significantly. That issue was easily resolved by increasing the force. Of more concern was the flaky appearance of the ISAM films around the edges of the pattern. The nanoimprinted features in (b) illustrated that significant shifting was occurring during the imprint process. Hence the sandwich method used in Phase 2 was not a sufficient mounting technique for ISAM films.

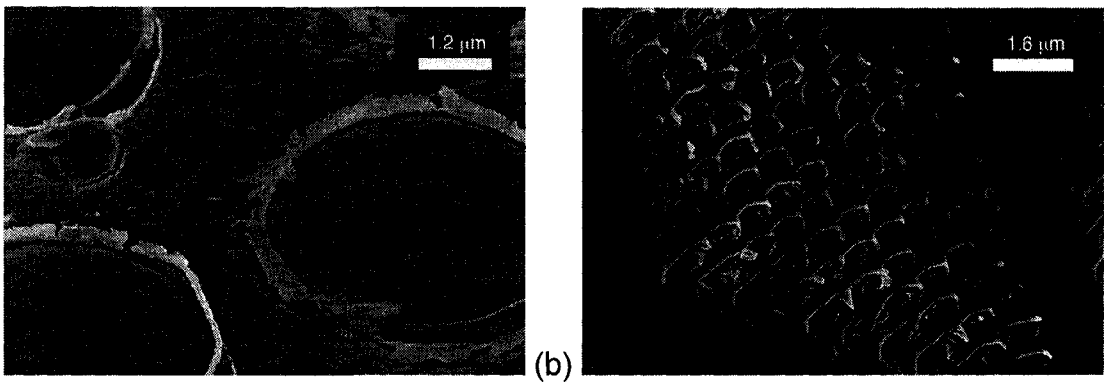

Figure 6.7: First imprint in ISAM films with a nanometer-scale silicon mold.

Finding an appropriate method of mounting both the mold and the substrate was essential to minimize this shifting. Various thin tapes were applied but later

rejected as the tape often contained pockets of air that would result in an uneven mounting. This lack of parallelity exposed certain points on both the mold and substrate to significant pressures that often led to mold and substrate fracture. A high temperature epoxy was found to be sufficiently thin that it enabled the mold and substrate to be mounted parallel with the embossing plates while preventing shifting.

Photonic crystal structures were imprinted into PCBS/PAH ISAM films as shown in Figure 6.8. The epoxy mounting technique eliminated the shifting seen previously, resulting in photonic crystals with an average hole diameter of 490 nm and a lattice spacing of 750 nm.

(a) 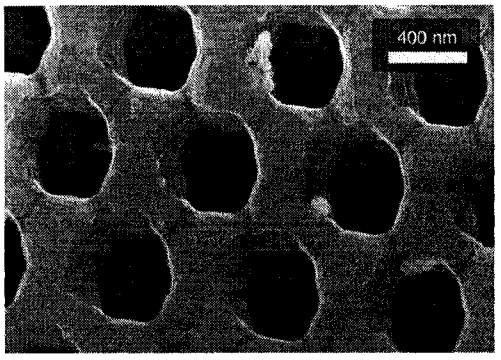

(b) 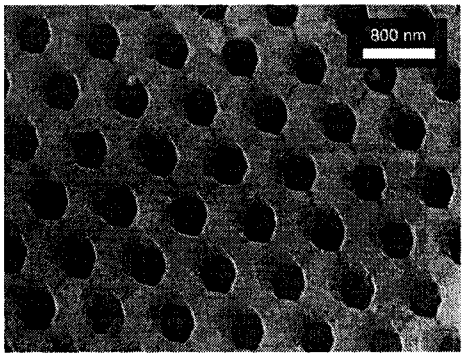

Figure 6.8: Photonic crystal structures imprinted in PCBS/PAH ISAM films with an average hole diameter of 490 nm and a lattice spacing of 750 nm.

Figure 6.9 shows 3 μm waveguide structures that were successfully imprinted into the ISAM films. Both a basic waveguide, (a) and waveguides with an integrated 620 nm period Bragg grating is shown in (b) and (c).

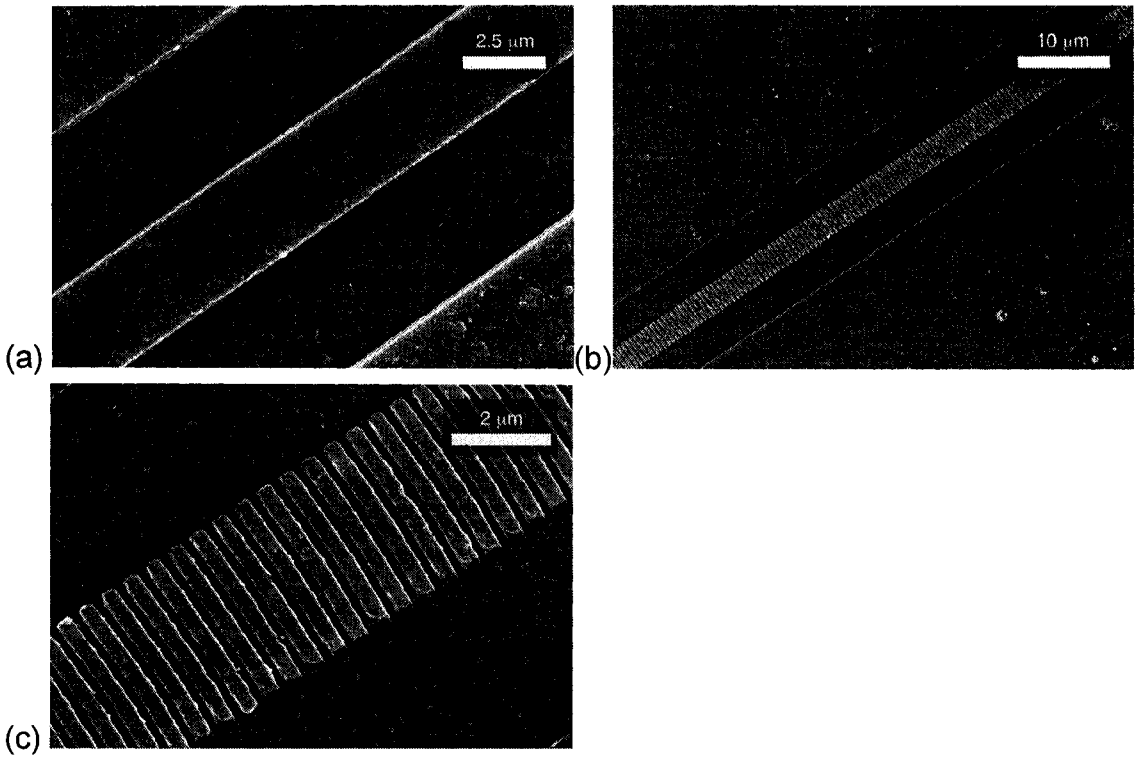

Figure 6.9: A basic waveguide (a) and a waveguide with an integrated Bragg grating, (b) and (c), were imprinted in ISAM films.

We were unable to conclusively demonstrate guiding in (a) because of insufficient transmitted power. It was expected that the transmitted power would be higher than that detected with reactive ion etched (RIE) patterned waveguides measured in Section 5.3. The significant decrease in sidewall roughness that results from eliminating the RIE step should result in a higher transmitted power because of the relatively smooth nanoimprinted walls. As before, the inhomogeneous sites contribute to the loss of transmitted power because they act like scatter sites. As well, the inhomogeneous sites result in incomplete imprinting because more time will be needed for sufficient polymer flow. Therefore, the molds do not penetrate the ISAM films completely (as seen in

Figure 6.10) which reduces the refractive index contrast making the waveguides more susceptible to scattering losses.

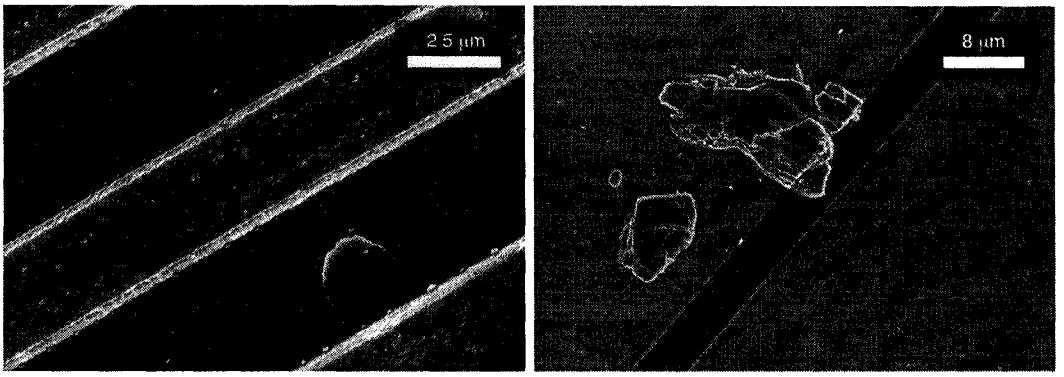

Figure 6.10: Demonstrations of incomplete imprinting because of inhomogeneous sites.

Preliminary x-ray photoelectron spectroscopy investigations presented in Section 4.4.2 indicated that exposure to typical nanoimprinting thermal cycles did not affect the composition of the PCBS/PAH ISAM films making the materials conducive to NIL patterning for mass production. Second harmonic generation (SHG) measurements were made to further determine whether exposure to the temperatures and forces involved in NIL would affect the ISAM films nonlinear optical behavior. The films were imprinted with molds with fill factors ranging from 0% (Control 1 and 2) to 25%, for a period of 2 h at 150°C and a pressure of 10 kN. This time was overshot to ensure complete polymer flow despite the presence of inhomogeneous sites. The films exhibit similar SHG results as shown in Figure. 6.11 after nanoimprinting, indicating again that the process is not adversely affecting their nonlinear optical response. Here the lines represent

the intensity measured at 532 nm (the second harmonic 1064 nm light).

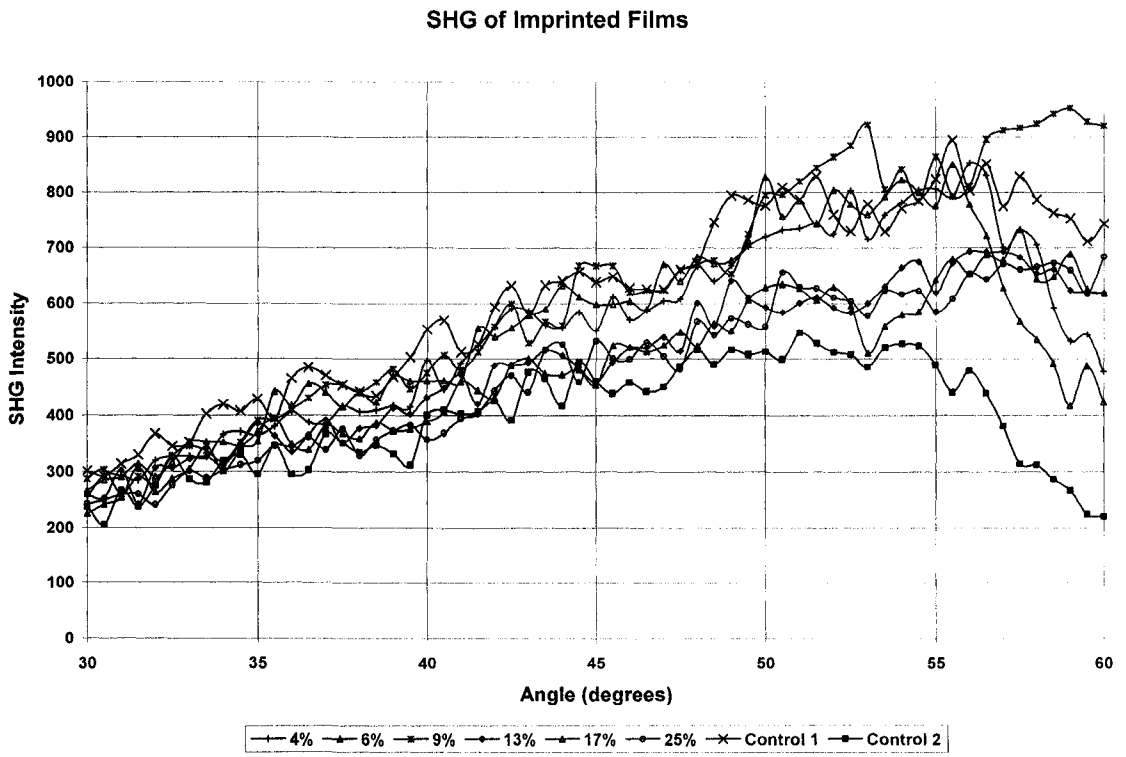

Figure 6.11: Second harmonic generation of PCBS/PAH ISAM films after being imprinted with different fill factors.

6.5 Summary

This chapter presented the fabrication technique for creating silicon molds and demonstrated photonic structures that were imprinted with nanoimprint lithography. To my knowledge, this is the first demonstration of patterning ISAM films with NIL. While further work needs to be done to remove the inhomogeneous sites, the success of imprinting ISAM films moves the field closer to a commercially viable pathway to ISAM photonic devices.

Chapter 7

Conclusion

This thesis presented a novel platform for the fabrication of nonlinear optical (NLO) photonic devices. Ionically self-assembled films are formed by alternately dipping a charged substrate into oppositely charged polyelectrolyte solutions. Because the bonding mechanism is electrostatic, ISAM films possess excellent thermal and temporal stability, maintaining their chromophore alignment without the need for poling. The primary goal was to develop a fabrication platform that would enable ISAM films to implemented in photonic devices. PCBS/PAH ISAM films were successfully patterned with reactive ion etching and nanoimprint lithography, which to my knowledge is the first such demonstration.

The ISAM films were electrostatically assembled from the NLO-active 10mM solution of PCBS polyanion at pH 7 and the NLO-inactive 10mM solution of PAH polycation at pH 7. AFM analysis characterized the films average roughness at 12.4 nm with peak height variation between 80 and 350 nm. These peak height variations can be attributed to inhomogeneous sites found within the films.

The thermal stability of these films was also investigated to determine their suitability for nanoimprint lithography. XPS investigations determined that the percent mass composition remained constant after undergoing thermal cycle that included heating the films to temperatures up to 200°C and then cooling them back to room temperature. Films that were exposed to the same thermal cycles possessed the same FTIR spectra, indicating that the bonding structure of the ISAM films were maintained after heating. Therefore, these thermal stability studies demonstrated PCBS/PAH were a suitable ISAM bilayer pair for NIL

A combination of electron beam lithography and reactive ion etching was used to pattern photonic structures in these films. An ISAM preheating treatment was developed to eliminate cracking in the films. Because the ISAM deposition technique involved aqueous solutions, trapped water in these films had to be removed before subsequent processing could occur. Protective layers were incorporated into the fabrication process to prevent ISAM film degradation. Both photonic crystals structures, with a lattice spacing of 710 nm and circle diameters ranging between 550 nm and 650 nm, and Bragg gratings, with a period of 570

nm, were successfully patterned with a combination of electron beam lithography and reactive ion etching. A hybrid ISAM/silicon fabrication technique was also presented as a method to increase the effective refractive index of the material for an enhanced photonic band gap effect while still maintaining the nonlinear optical benefits of the ISAM films.

Nanoimprint lithography of ISAM films was chosen as a method to pattern ISAM films by leveraging their inherent polymeric nature. Silicon molds were fabricated with deep silicon etching and passivated with a silane monolayer to prevent polymer adhesion. A proper mounting technique was developed to prevent both shifting during nanoimprinting and to enhance the parallelity of the mold and substrate to prevent their cracking with increased force. Photonic crystals, with an average hole diameter of 490 nm and a lattice spacing of 750, and Bragg gratings, with a period of 620 nm, were fabricated using nanoimprint lithography.

The second harmonic generation signal was also measured on ISAM films imprinted with fill factors ranging between 0 to 25%. It was determined that nanoimprinting does not adversely affect the nonlinear optical behavior of PCBS/PAH ISAM films, further indicating their suitability for nanoimprinting.

Measurements of transmitted power from a simple waveguide created with the reactive ion etch method indicated that guiding was occurring. The loss in transmitted power can be attributed to the scattering effect of inhomogenous

sites found in the ISAM films as well as the rough sidewalls. These rough walls were a combined result of the chrome etch and the plasma etch process. Because nanoimprint lithography results in smoother sidewalls, it was believed that the transmitted power measured in the nanomprinted waveguides should have been higher than the reactive ion etched waveguides. Unfortunately, a conclusive demonstration of guiding in imprinted waveguides could not be realized. Inhomogeneous sites in the ISAM films prevent complete nanoimprinting from occurring because of the increased time needed for polymer flow. Thus with incomplete imprinting, the refractive index contrast was decreased thereby increasing the sensitivity to the scattering effect of the inhomogeneous sights.

We anticipate that the further development of these fabrication techniques will encourage more patterning of ISAM films, whether it be patterning hybrid ISAM/covalent films that posses a stronger nonlinear optical behavior for photonic devices, or patterning ISAM films with different functionalities. At the very least, it is expected that this work should provide more fabrication solutions as workable options for creating structures in ISAM films.

Future Work

Several directions could be taken to further improve this work. Differential scanning calorimetry would be useful for determining the glass transition temperature of PCBS/PAH ISAM films. Because ISAM films are an electrostatic

buildup of oppositely charged monolayers and not a simple polymer, their glass transition temperature is expected to be different then either PCBS or PAH by themselves.

Investigation on methods to eradicate the inhomogeneous sites is necessary for practical integration of nonlinear optical ISAM films. Eliminating any pre-existing contamination or roughness of the substrates would decrease contamination. Therefore ISAM films should only be deposited on silicon and optical quality glass in the future. Since submicron filtering of the solutions before deposition did not result in a noticeable decrease in inhomogeneous sites, they are most likely not a result of contamination before deposition. More frequent changing of the solutions appears to be an obvious solution to reduce particulates or potential build up of cross contamination. Ultrasonic agitation of the polyelectrolyte baths has been demonstrated as a method to reduce patchy film growth [10] and might contribute to the creation of smoother films by preventing either particulates or perhaps agglomerates (if a small degree of cross contamination is occurring) from forming a stable electrostatic bond with the substrate.

Photonic structures could then be tested upon removal of these inhomogeneous sites because scattering should be significantly reduced. Demonstration of wavelength filtering with a simple nanoimprinted Bragg grating would indicate ISAM films' suitability in practical photonic devices. It would therefore be straightforward to demonstrate the Pockels effect by nanoimprinting a Mach-

Zehnder interferometer into the ISAM films. By placing electrodes above and below one arm of the interferometer, a phase change could be induced in light traveling in that arm, resulting in constructive and destructive interference when the arms recombined.

Bibliography

[1] J.R. Heflin, C. Durak, P.J. Neyman, C. Brands, M.T. Guzy, K. Gaskins, A. Garg, RM. Davis, KE. Van Cott, H. Wang, and H.W. Gibson, "Organic Electro-optic Films Fabricated by Hybrid Covalent/Ionic Self-Assembly," Conference on Lasers & Electro-Optics, vol. 3, pp. 1864- 1866, 2005.

[2] J.R. Heflin, Y. Liu, C. Figura, D. Marciu, and R.O. Claus, "Second Order Nonlinear Optical Thin Films Fabricated from Ionically Self-Assembled Monolayers," Proceedings of SPIE, vol. 3147, pp. 10-19, 1998.

[3] H. Schift1, S. Park, B. Jung,C. Choi, C. Kee, S. Han, K. Yoon, and Jens Gobrecht, "Fabrication of polymer photonic crystalsusing nanoimprint lithography," Nanotechnology, vol. 16, pp. S261–S265, 2005.

[4] Y. Chou, P. R. Krauss, W. Zhang, L. J. Guo, and L. Zhuang, "Sub-10 nm imprint lithography and applications," J. Vac. Sci. Technol. B, vol. 15, no. 6, pp. 2897-2904, 1997

[5] L.J. Guo, "Recent progress in nanoimprint technology and its applications," Journal of Physics D: Applied Physics, vol. 37, pp R123-R141, 2004.

[6] C. Chao and L.J Guo, "Polymer microring resonators fabricated by nanoimprint technique," J. Vac. Sci. Technol. B, vol. 20, no..6, pp. 2862-2866, 2002.

[7] W. Jiang, Y. Jiang, L. Gu, L. Wang, X. Chen, and R.T. Chen, "Silicon and polymer nanophotonic devices based on photonic crystals," Proceedings. Of SPIE, vol. 6124, 612410-1, 2006.

[8] D. Pisignano, L. Persano, G. Gigli, P.Visconti, T. Stomeo, M. De Vittorio, G. Barbarella, L. Favaretto, and R. Cingolani, "Planar organic photonic crystals fabricated by soft lithography," Nanotechnology, vol. 15, pp. 766-770, 2004.

[9] M. Eich, G.C. Biorklund, and D.Y. Yoon, "Poled Amorphous Polymers for Second-Order Nonlinear Optics," Polymers for Advanced Technologies, vol. , pp. 189-198, 1990.

[10] X. Cheng and L.J. Guo, "Electrostatic self assembly of nanocomposite polymers in grating Structures," J. Vac. Sci. Technol. B, vol. 19, no..6, pp. 2736-2740, 2001.

[11] S.K. Yesodha, C.K. Sadashiva Pillai, N. Tsutsumi, "Stable polymeric materials for nonlinear optics: a review based on azobenzene systems," Prog. Polym. Sci, vol. 29, pp. 45–74, 2004.

[12] H. Kimura-Suda , Y. Zhang , T. Sassa , T. Wada , and H. Sasabe, "Polar Alignment in Spin-Coated Carbazole Main- and Side-Chain Polymer Films," Advanced Materials, vol. 12, no. 16, pp. 1196 – 1199, 2000.

[13] K.E. Van Cott, M. Guzy, P. Neyman, C. Brands, J.R. Heflin, and H.W. Gibson, and R.M. Davis, "Layer-By-Layer Deposition and Ordering of Low-Molecular-Weight Dye Molecules for Second-Order Nonlinear Optics," Angew. Chem. Int. Ed., vol. 41, no. 17, pp. 3235-3238, 2002.

[14] C. Figura, P. Neyman, D. Marciu, C. Brands, M.A. Murray, S. Hair, R.M. Davis, M.B. Miller, and J.R. Heflin, "Thermal Stability and Immersion Solution Dependence of Second Order Nonlinear Optical Ionically Self-Assembled Films," Proceedings of SPIE , vol. 3939, pp 214-222, 2000.

[15] R.P. Bertram, N. Benter, D. Apitz, E. Soergel, K. Buse, R. Hagen and S.G. Kostromine, "Increased thermal stability of a poled electro-optic polymer using high-molar-mass fractions," Physical Review E, vol. 70, 041802, 2004.

[16] R.D. Schaller, R.J. Saykally, Y.R. Shen, and F. Lagugné-Labarthet, "Poled polymer thin-film gratings studied with far-field optical diffraction and second-harmonic near-field microscopy, Optics Letters, vol. 28, no. 15, pp.1296-1298, 2003.

[17] X. Ni, M. Nakanishi, O. Sugihara, and N. Okamato, "Fabrication of $x^{(2)}$ Grating in Poled Polymer Waveguide Based on Direct Laser Beam Writing," Optical Review, vol. 5, no. 1, pp. 9-11, 1998.

[18] J. Zhou, A. Pyayt, L.R. Dalton, J. Luo, A.K.Y. Jen, and A. Chen, "Photobleaching Fabrication of Microring Resonator in a Chromophore-Containing Polymer," IEEE Photonics Technology Letters, vol. 18, no. 21, pp. 2221-2223, 2006.

[19] S. Lee, O. Kwon, Y.Won, and D. Cho, "Micro-patterned Domain Structures of Nonlinear Optical Side-group Polymers by Corona Poling," Jpn. J. Appl. Phys., vol. 41, pp. 5235–5236, 2002.

[20] R. Mustacich, M. Gilbert, R. Finn, and C. Swann, "Analysis and fabrication of overlapping-electrode designs for poling and modulating channels in polymer thin films," Applied Optics, vol. 31, no. 15, pp. 2800-2806, 1992.

[21] O. Sugihara, Y. Che, N. Okamoto, H. Fujimura, C. Egami, and S. Umegaki, "High-resolution periodically poled structure in diazo-dye-substituted polymer film based on direct electron-beam writing technique," Applied Physics Letters, vol. 73, no. 21, pp. 3028-3030, 1998.

[22] S. Ahn and S. Shin, "Grating-assisted codirectional coupler filter using electro-optic and passive polymer waveguides," Optics Communications, vol. 197, pp. 289-293, 2001.

[23] S. Lee and S. Shin, "Polarisation-insensitive digital optical switch using an electro-optic polymer rib waveguide," Electronics Letters, vol. 33, no. 4, pp. 314-316, 1997.

[24] H. Kimura-Suda, Y. Zhang, T. Sassa, T. Wada, and H. Sasabe, "Polar Alignment in Spin-Coated Carbazole Main- and Side-Chain Polymer Films," Advanced Materials, vol. 12, no. 16, pp. 1196-1199, 2000.

[25] O. Sugihara, M. Nakanishi, H. Fujimura, C. Egami, and N. Okamoto, "Simultaneous process of embossing and poling at elevated temperatures: a simple technique for nonlinear grating formation in polymer films, Optics Letters, vol. 25, no. 14, pp. 1028-1030, 2000.

[26] Z. Wang, J.R. Heflin, R.H. Stolen, and S. Ramachandran, "Highly sensitive optical response of optical fiber long period gratings to nanometer-thick ionic self-assembled multilayers," Applied Physics Letters, vol. 86, 223104, 2005.

[27] O.N. Oliveira Jr., D.S. dos Santos Jr., D.T. Balogh, V. Zucolotto, and C.R. Mendonca, "Optical storage and surface-relief gratings in azobenzene-containing nanostructured films, Advances in Colloid and Interface Science, vol. 116, pp. 179 – 192, 2005.

[28] H. Kim, H. Shin, J. Ha, M. Lee, and K. Lim, "Optical patterning of silver nanoparticle Langmuir-Blodgett films," Journal of Applied Physics, vol. 102, 083505, 2007.

[29] G.G. Roberts, "An applied science perspective of Langmuir-Blodgett films," Advances in Physics, vol. 34, no. 4, pp. 475-512, 1985.

[30] G.J. Ashwell, "Langmuir–Blodgett films: molecular engineering of non-centrosymmetric structures for second-order nonlinear optical applications, J. Mater. Chem., vol. 9, pp. 1991-2003, 1999.

[31] G. Decher, "Fuzzy Nanoassemblies: Toward Layered Polymeric Multicomposites, Science, vol. 277, pp. 1232-1237, 1997.

[32] J.A. Zasadzinski; R. Viswanthan; L. Madsen; J. Garnaes; and D.K. Schwartz, "Langmuir-Blodgett Films," *Science*, vol. 263, no. 5154, pp. 1726-1733, 1994.

[33] Y. Liu, A. Rosidian, K. Lenahan, Y. Wang, T. Zeng, and R.O. Claus, "Characterization of electrostatically self-assembled nanocomposite thin films, Smart Mater. Struct., vol.8, pp. 100-105, 1999.

[34] D.Y. Takamoto, E. Aydil, J.A. Zasadzinski, A.T. Ivanova, D.K. Schwartz, T. Yang, and P.S. Cremer, "Stable Ordering in Langmuir-Blodgett Films", Science, vol. 293, pp. 1292-1295, 2001.

[35] D.L. Allara, "Critical issues in applications of selfassembled monolayers," Biosensors & Bioelectronics,vol. 10, pp. 771-783, 1995.

[36] H.C. Day, D.R. Allee, R. George, and V.A. Burrows, "Nanometer scale patterning of a monolayer Langmuir-Blodgett film with a scanning tunneling microscope in air," Appl. Phys. Lett., vol. 62, no. 14, pp. 1629-1631, 1993.

[37] M. Hirtz, H. Fuchs, and L. Chi, "Influence of Substrate Treatment on Self-Organized Pattern Formation by Langmuir-Blodgett Transfer," J. Phys. Chem. B, 2007.

[38] S. Lenhert, L. Zhang, J. Mueller, H.P. Wiesmann, G. Erker, H. Fuchs, L. Chi, "Self-Organized Complex Patterning: Langmuir-Blodgett Lithography," Advanced Materials, vol. 16, no. 7, pp. 619-624, 2004.

[39] T. Li, M. Mitsuishi, and T. Miyashita, "Fabrication of Nanometer Scale Patterns with Polymer Langmuir-Blodgett Films," Azojomo, vol. 2, pp. 1-9, 2006.

[40] Q. Guo, X. Teng, H. Yang, "Fabrication of Magnetic FePt Patterns from Langmuir-Blodgett Films of Platinum-Iron Oxide Core-Shell Nanoparticles," Advanced Materials, vol. 16, no. 15, pp. 1337-1341, 2004.

[41] R. Paolesse, C. Di Natale, A. Macagnano, F. Davide, T. Boschi, and A. D'Amico, "Self-assembled monolayers of mercaptoporphyrins as sensing material for quartz crystal microbalance chemical sensors," Sensors and Actuators B, vol. 47, pp. 70–76, 1998.

[42] S. Stockhause, P. Neumann, S. Schrader, M. Kant, and L. Brehmer, "Structural and optical properties of self-assembled multilayers based on organic zirconium bisphosphonates," Synthetic Metals, vol. 127, no. 1-3, pp. 295-298, 2002.

[43] W. Lin, W. Lin, G.K. Wong, and T.J. Marks, "Supramolecular Approaches to Second-Order Nonlinear Optical Materials. Self-Assembly and Microstructural Characterization of Intrinsically Acentric [(Aminophenyl)azo]pyridinium Superlattices," J. Am. Chem. Soc., vol. 118, pp. 8034-8042, 1996.

[44] T. Wink, S.J. van Zuilen, A. Bult, and W.P. van Bennekom, "Self-assembled Monolayers for Biosensors," Analyst, vol. 122, pp. 43R-50R, 1997.

[45] J.L. Wilbur, A. Kumar, E. Kim, G.M. Whitesides, "Microfabrication by microcontact printing of self-assembled monolayers," Advanced Materials, vol. 6, no. 7-8, pp. 600-604, 2004.

[46] J.L Wilbur, A. Kumar, H.A. Biebuyck, E. Kim, and G.M. Whitesides, "Microcontact printing of self-assembled monolayers: applications in microfabrication," Nanotechnology, vol. 7, pp. 452-457, 1996.

[47] L. Yan, X. Zhao, and G.M. Whitesides, "Patterning a Preformed, Reactive SAM Using Microcontact Printing," J. Am. Chem. Soc., vol.120, no. 24, pp. 6179 -6180, 1998.

[48] G. Liu, S. Xu, AND Y. Qian, "Nanofabrication of Self-Assembled Monolayers Using Scanning Probe Lithography, Acc. Chem. Res., vol. 33, pp. 457-466, 2000.

[49] M.J. Lercel, H.G. Craighead, A.N. Parikh, K. Seshadri, and D.L. Allara, "Sub-10 nm lithography with self-assembled monolayers," Appl. Phys. Lett., vol. 68, vol. 11, pp. 1504-1506, 1996.

[50] G. Purvinis, P.S. Priambodo. M. Pomerantz, M. Zhou, T.A. Maldonado, and Robert Magnusson, "Second-harmonic generation in resonant waveguide gratings incorporating ionic self-assembled monolayer polymer films," Optics Letters, vol. 29, no.10, pp. 1108-1110, 2004.

[51] F.J. Arregui, B. Dickerson, R.O. Claus, I.R. Matias, and K.L. Cooper, "Polymeric Thin Films of Controlled Complex Refractive Index Formed by the Electrostatic Self-Assembled Monolayer Process," IEEE Photonics Technology Letters, vol. 13, no. 12, pp. 1319-1321, 2001.

[52] D. Marciu, M. Miller, A.L. Ritter, M.A. Murray, P.J. Neyman, W. Graupner, J.R. Heflin, H. Wang, H.W. Gibson, and R.M. Davis, "Efficiency Optimization in Ionically Self-Assembled Thin Film Polymer Light-Emitting Diodes," Proceedings of SPIE, vol. 3938, pp. 169-179, 2000.

[53] P.T. Hammond. "Recent explorations in electrostatic multilayer thin film assembly," Current Opinion in Colloid & Interface Science, vol. 4, pp. 430-442, 2000.

[54] J.R. Heflin, M.T. Guzy, P.J. Neyman, K.J. Gaskins, C. Brands, Z. Wang, H.W. Gibson, R.M. Davis, and K.E. Van Cott, "Efficient, Thermally Stable, Second

Order Nonlinear Optical Response in Organic Hybrid Covalent/Ionic Self-Assembled Films," Langmuir, vol. 22, pp. 5723-5727, 2006.

[33] F. Shi, B. Dong, D. Qiu, J. Sun, T. Wu, and X. Zhang, "Layer-by-Layer Self-Assembly of Reactive Polyelectrolytes for Robust Multilayer Patterning,"Adv. Mater., vol. 14, no. 11, pp. 805-809, 2002.

[56] A. Rosidian, Y. Liu, and R.O. Claus, "Ionic Self-Assembly of Ultrahard ZrO2/Polymer Nanocomposite Thin Films," Adv. Mater., vol. 10, no. 14, pp. 1087-1091, 1998.

[57] F.J. Arregui, I.R. Matias, K.L. Cooper, and R.O. Claus, "Fabrication of micrograting on the ends of standard optical fibers by the electrostatic self-assembly monolayer process," Optics Letters, vol. 26, no. 3, pp. 131-133, 2001.

[58] K. Hyde, M. Rusa, and J. Hinestroza, "Layer-by-layer deposition of polyelectrolyte nanolayers on natural fibres: cotton," Nanotechnology, vol. 16, pp. S422-S428, 2005.

[59] D.A. Chang-Yen and B.K. Gale, "An Integrated Optical Biochemical Sensor Fabricated Using Rapid-Prototyping Techniques," Lab Chip, vol. 3, pp. 297-301, 2003.

[60] Y. Liu, W.i Zhao, Y. Wang, and R.O. Claus, "Functionally-Tailored Nanoparticle-Based Tonically Self-Assembled Multi-layer Thin-Films," SPIE, vol. 3324, pp. 45-48, 1998.

[61] P.J. Neyman, M. Guzy, S.M. Shah, R.M. Davis, K.E.Van Cott, H.Wang, H.W. Gibson, C. Brands, and J.R. Heflin, "Novel Hybrid Covalent / Ionic Self-Assembly Technique for Improved Second-Order Nonlinear Optical Films," Mat. Res. Soc. Symp. Proc., vol. 708, pp. BB4.4.1-BB4.4.6, 2002.

[62] C. Brands, P.J. Neyman, M.T. Guzy, S. Shah, K.E. Van Cott, R.M. Davis, H. Wang, H.W. Gibson, and J.R. Heflin, "In Situ Second Harmonic Generation Measurements of the Growth of Nonlinear Optical Ionically Self-assembled Monolayers." Mat. Res. Soc. Symp. Proc., vol. 660, pp. JJ8.32.1-JJ8.32.6, 2001.

[63] H. Shibru, Y. Zhang, K.L. Cooper, G.R. Pickrell, and Anbo Wang, "Optimization of layer-by-layer electrostatic self-assembly processing parameters for optical biosensing," Optical Engineering, vol. 45, no. 2, 024401, 2006.

[64] J.R. Heflin, C. Figura, D. Marciu, Y. Liu, and R.O. Claus, "Thickness dependence of second-harmonic generation in thin films fabricated from ionically self-assembled monolayers" Applied Physics Letters, vol. 74, no. 4, pp. 495-497, 1999.

[65] K. Chen, C. Durak, J.R. Heflin, and H.D. Robinson, "Plasmon-Enhanced Second-Harmonic Generation from Ionic Self-Assembled Multilayer Films," Nano Letters, vol. 7, no. 2, pp. 254-258, 2007.

[66] Y. Lvov, G. Decher, and H. Mohwald, "Assembly, Structural Characterization, and Thermal Behavior of Layer-by-Layer Deposited Ultrathin Films of Poly(vinyl sulfate) and Poly(allylamine)," Langmuir, vol. 9, pp. 481-486, 1993.

[67] G. Decher, J.D. Hong, and J. Schmitt, "Buildup of ultrathin multilayer films by a self-assembly process: III. Consecutively alternating adsorption of anionic and cationic polyelectrolytes on charged surfaces," Thin Solid Films, vol. 210/211, pp. 831-835, 1992.

[68] Y. Lvov, G. Decher, and G. Sukhorukov, "Assembly of Thin Films by Means of Successive Deposition of Alternate Layers of DNA and Poly(ally1amine)," Macromolecules, vol. 26, pp. 5396-5399, 1993.

[69] J. Ji and J. Shen, Electrostatic Self-assemble and Nanomedicine," Proceedings of the 2005 IEEE, pp. 720-722, 2005.

[70] D. Kommireddy, J. Shi, X. Yan, H. Ji, and Y. Lvov, "Electrostatic Layer-by-Layer Nano-Assembly: Films, Cantilevers, Micropatterns and Nanocapsules," Proceedings of SPIE, vol. 4492, pp. 120-131, 2005.

[71] H. Wei and E. Wang, "Electrochemiluminescence-based DNA Detection Using Guanine Oxidation at Electrostatic Self-assembly of Ru(bpy)3 2*p*-doped Silica Nanoparticles on Indium Tin Oxide Electrode," Chemistry Letters, vol. 36, no. 2, pp. 210-211, 2007.

[72] T.R. Farhat and J. B. Schlenoff, "Corrosion Control Using Polyelectrolyte Multilayers," *Electrochemical and Solid-State Letters*, vol. 5, no. 4, pp. B13-B15, 2002.

[73] D. Marciu, M.B. Miller, C. Kozikowski, J.R. Heflin, S. Cho, B.A.Reid, K. Kuroda, W. Graupner, H. Wang, H.W. Gibson, and R.M. Davis, "Enhanced Photovoltaic Response in Ionically Self-Assembled Monolayer Thin-Film Devices," Mat. Res. Symp. Proc., vol. 708, pp. BB9.4.1-BB9.4.7, 2002.

[74] B. Pradhan, A. Bandyopadhyay, and A.J Pal, "Molecular level control of donor/acceptor heterostructures in organic photovoltaic devices," Applied Physics Letters, vol. 85, no. 4, pp. 663-665, 2004.

[75] J.A. Janik, J.R. Heflin, D. Marciu, M.B. Miller, and R.M. Davis3, "Electrochromic Behavior of Ionically Self-Assembled Thin Films," Mat. Res. Soc. Symp. Proc., vol 660, pp. JJ8.20.1-JJ8.20.6, 2001.

[76] T Zeng, R Claus, Y Liu, F Zhang, W Du, and K L Cooper, "Piezoelectric ultrathin polymer films synthesized by electrostatic self-assembly processing,"Smart Mater. Struct., vol. 9, pp. 801-804, 2000.

[77] S. E. Yancey, W. Zhong, J. R. Heflin, and A. L. Ritter, "The influence of void space on antireflection coatings of silica nanoparticle self-assembled films," Journal of Applied Physics, vol 99, 034313, 2006.

[78] L. Chen, X, Tian, L. Tian. L. Liu, W. Song, and H. Xu, " Electrochemical reduction and flow detection of iodate on (Bu4N)2Mo6O19 self-assembled monolayer," Anal Bioanal Chem, vol. 382, pp. 1187-1195, 2005.

[79] F.J. Arregui, K.L. Cooper, Y. Liu, I.R. Matias, and R.O. Claus, "Optical Fiber Humidity Sensor with a Fast Response Time Using the Ionic Self-Assembly Method," ICICE Trans. Electron., vol. E83-C, no. 3, pp. 360-365, 2000.

[80] J.M. Corres, J. Bravo, and I.R. Matias, "Nonadiabatic Tapered Single-Mode Fiber Coated With Humidity Sensitive Nanofilms," IEEE Photonics Technology Letters, vol. 18, no. 8, pp. 935-937, 2006.

[81] F.J. Arregui, I. Latasa, I.R. Matias, and R.O. Claus "An optical fiber pH sensor based.on the electrostatic self-assembly method," Proceedings of IEEE, vol. 1, pp. 107-110, 2003.

[82] Z. Wang, J.R. Heflin, K. Vancott, R.H. Stolen, S. Ramachandran, and S. Ghalmi, "Ionic Self-Assembled Multilayers Adsorbed on Long Period Fiber Gratings for Use as Biosensors," Conference on Laser and Electro-Optics, vol. 3, pp. 1683-1685, 2005.

[83] K. Cai, Y. Hu, K.D. Jandt, and Y. Wang, "Surface modification of titanium thin film with chitosan via electrostatic self-assembly technique and its influence on osteoblast growth behavior," J Mater Sci, 2007.

[84] H. Zhu, J Ji, M.A. Barbosa, and J. Shen, "Protein Electrostatic Self-Assembly on Poly(DL-Lactide) Scaffold to Promote Osteoblast Growth," J Biomed Mater Res Pt B Appl Biomater, vol. 71B, no. 1, pp. 159-165, 2004.

[85] P. Bertrand, A. Jona1, A. Laschewsky, and R. Legras, "Ultrathin polymer coatings by complexation of polyelectrolytes at interfaces: suitable materials, structure and properties," Macromol. Rapid Commun, vol. 21, pp. 319-348, 2000.

[86] T. Cao, F. Wei, X. Jiao, J. Chen, W. Liao, X Zhao, and W. Cao, "Micropatterns of Protein and Conducting Polymer Molecules Fabricated by Layer-by-Layer Self-Assembly and Photolithography Techniques," Langmuir, vol. 19, pp. 8127-8129, 2003.

[87] C.S. Camilo, D.S. dos Santos, Jr., J.J. Rodrigues, Jr., M.L. Vega, S.P. Campana Filho, O.N. Oliveira, Jr., and C. R. Mendoncüa, "Surface-Relief Gratings and Photoinduced Birefringence in Layer-by-Layer Films of Chitosan and an Azopolymer," Biomacromolecules, vol. 4, pp. *1583-1588, 2003.*

[88] *Y. Lin, C. Jiang, J. Xu, Z. Lin,* and *V.V. Tsukruk, "*Sculptured Layer-by-Layer Films," Adv. Mater., vol. 19, pp. 3827-3832, 2007.

[89] D. Wang, A.L. Rogach, and F. Caruso, "Composite Photonic Crystals from Semiconductor Nanocrystal/Polyelectrolyte-Coated Colloidal Spheres," Chem. Mater., vol. 15, pp. 2724-2729, 2003.

[90] J. Coates, "Interpretation of Infrared Spectra, A Practical Approach,"Encyclopedia of Analytical Chemistry, pp. 10815-10837, 2000.

[91] V. Zucolotto, M. Ferreira, M.R. Cordeiro, C.J.L. Constantino, D.T. Balogh, A.R. Zanatta, W.C. Moreira, and O.N. Oliveira Jr., "Unusual Interactions Binding Iron Tetrasulfonated Phthalocyanine and Poly(allylamine hydrochloride) in Layer-by-Layer Films," J. Phys. Chem. B, vol. 107, pp. 3733-3737, 2003.

[92] D.W. Hoffman, "Perspective on stresses in magnetron-sputtered thin films," J. Vac. Sci. Technol. A, vol. 12, no. 4, pp. 953-961, 1994.

[93] Y. Zhao, F. Wang, Z.C. Cui, J. Zheng, H.M. Zhang, D.M. Zhang, S.Y. Liu, and M.B. Yi, "Study of reactive ion etching process to fabricate the PMMA-based polymer waveguide," Microelectronics Journal, vol. 35, pp. 605-608, 2004.